STRESS CONCENTRATIONS AROUND A SQUARE CUTOUT IN A COMPOSITE PLATE

by

COLIN P. CANNON

Presented to the Faculty of the Graduate School of
The University of Texas at Arlington in Partial Fulfillment
of the Requirements
for the Degree of

MASTER OF SCIENCE IN AEROSPACE ENGINEERING

THE UNIVERSITY OF TEXAS AT ARLINGTON
December 2012

ACKNOWLEDGEMENTS

I would like to sincerely thank my advisor, Dr. Wen Chan, for his guidance and patience. Without his help it would not have been possible for me to achieve my goals and develop into the engineer that I have become.

I would also like to thank my parents and my sister for their love and support throughout the many years of school. They set an example of a determined work ethic and encouraged me to strive to do my best.

Most of all, I would like to thank my wife for her love and sacrifice during these challenging times. She is my motivation and my drive and without her support day to day, I would not have been able to complete such an accomplishment.

November 26, 2012

ABSTRACT

STRESS CONCENTRATIONS AROUND A SQUARE

CUTOUT IN A COMPOSITE PLATE

Colin Cannon, M.S.

The University of Texas at Arlington, 2012

Supervising Professor: Wen Chan

Composite structure in the aircraft industry has been in development for well over half a century and yet the understanding of the effects of a square cutout is generally limited to quasi-isotropic laminates. Currently, the closed-form solution to calculate the stresses around a cutout is limited to symmetric anisotropic laminates with limitations on the cutout shapes.

Finite Element Analysis, using MSC PATRAN and NASTRAN, was performed on 2D composite laminates containing square cutouts with rounded corners. The laminate stacking sequence was varied from symmetric and balanced to unsymmetric and unbalanced and the square cutouts each had different radii at the corners. The stress concentration factors from a uniaxial load were identified at the laminate and the lamina level. The effects of the stacking sequence and the varying radii were identified to better understand the physics of a square cutout in a composite plate.

TABLE OF CONTENTS

ACKNOWLEDGEMENTS iii

ABSTRACT iv

LIST OF ILLUSTRATIONS viii

LIST OF TABLES x

NOMENCLATURE xii

Chapter Page

1. INTRODUCTION 1

1.1 Composite Overview 1

1.1.1 Historical Uses 1

1.1.2 Composite Materials 4

1.1.3 Laminate Properties 6

1.2 Cutouts 7

1.3 Thesis Overview 8

1.3.1 Thesis Objectives 8

1.3.2 Chapter Layout 8

2. LITERATURE REVIEW 9

2.1 Stress Concentrations in Metallics 9

2.2 Stress Concentrations in Composites 9

3. FINITE ELEMENT MODEL GENERATION AND VALIDATION 14

3.1 Geometry and Material 14

3.1.1 Plate Configurations 14

3.1.2 Lamina and Laminate Properties 15

3.2 Model Generation 16

3.2.1 NASTRAN Properties 16
3.2.2 Meshing 17
3.2.3 Boundary Conditions and Applied Loads 21
3.2.4 Numbering Scheme 22
3.3 Obtaining Results 24
3.3.1 Controlled Output 24
3.3.2 Processing Data 24
3.4 Validation 25
3.4.1 Isotropic Plate 25
4. ANALYTICAL RESULTS 26
4.1 Composites Analysis Review 26
4.1.1 Macromechanics 26
4.1.2 Classical Lamination Theory 28
4.2 Stress Concentrations 31
4.2.1 Isotropic Plate 31
4.2.2 Anisotropic Plate 33
4.3 Laminate Analysis 41
4.3.1 Circular Cutout 41
5. NUMERICAL RESULTS 43
5.1 Lekhnitskii Validation 43
5.2 Laminate Based Stress Concentration Factors 44
5.2.1 Results – Circular Cutout 45
5.2.2 Results – Square Cutout with Corner Radius of 0.4 inches 46
5.2.3 Results – Square Cutout with Corner Radius of 0.3 inches 47
5.2.4 Results – Square Cutout with Corner Radius of 0.2 inches 48

5.2.5 Results – Square Cutout with Corner Radius of 0.1 inches 49
5.2.6 Summary of Cutouts 50
5.3 Lamina Based Stress Concentration Factors – Fiber Stress 55
5.3.1 Results – Circular Cutout 56
5.3.2 Results – Square Cutout with Corner Radius of 0.4 inches 57
5.3.3 Results – Square Cutout with Corner Radius of 0.3 inches 58
5.3.4 Results – Square Cutout with Corner Radius of 0.2 inches 59
5.3.5 Results – Square Cutout with Corner Radius of 0.1 inches 60
5.3.6 Summary of Cutouts 61
5.4 Stress Distribution 66
6. CONCLUSION 69
APPENDIX
A. LEKHNITSKII'S FORMALISM IN A MATHCAD TEMPLATE 71
REFERENCES 75
BIOGRAPHICAL INFORMATION 77

LIST OF ILLUSTRATIONS

Figure Page

1.1 SR-71 Use of Composite Materials 2

1.2 Boeing 787 Developmental Fuselage Section 3

1.3 Continuous Fiber-Reinforced Lamina Definition 4

1.4 Laminate Stack-Up Definition 6

3.1 Plate Dimensions 14

3.2 Sample PCOMPG Card of $[0/\pm45/90]_s$ 16

3.3 FEM Surfaces of Plate with Square Cutout (r=0.3") 18

3.4 (a) Mesh Seeding for Model 3, (b) Mesh Seeding for Corner of Model 3 with Mesh 19

3.5 Plate Model with Mesh for Square Cutout 20

3.6 CBUSH Elements and Distributed Loads 21

3.7 Corner Elements Numbering Order (See Table 3.7) 23

3.8 Displacement Node Numbering Order 23

4.1 Stress-Strain Relation in a Laminate 28

4.2 Element of Single Layer with Force and Moment Resultants 29

4.3 Laminate Plate Geometry and Numbering Scheme 30

4.4 Plate Geometry and Loading Configuration 35

4.5 Global X-Direction Stress Along Cutout Boundary $[0/\pm45/90]_s$ 37

4.6 Mapping Function – Square (λ=0.707, w=0.075, n=3, c=1) 39

4.7 Mapping Function – Square (λ=0.707, w=0.1, n=3, c=1) 40

4.8 Mapping Function – Square (λ=0.707, w=0.125, n=3, c=1) 40

5.1 Laminate SCF – Quasi-Isotropic Laminates 50

5.2 Laminate SCF – Orthotropic Laminates 51

5.3 Laminate SCF – Symmetric Anisotropic Laminates 52
5.4 Laminate SCF – Unsymmetric Laminates 53
5.5 Laminate SCF – Antisymmetric Laminates 54
5.6 Lamina SCF – Quasi-Isotropic Laminates 61
5.7 Lamina SCF – Orthotropic Laminates 62
5.8 Lamina SCF – Symmetric Anisotropic Laminates 63
5.9 Lamina SCF – Unsymmetric Laminates 64
5.10 Lamina SCF – Antisymmetric Laminates 65
5.11 Stress Distribution for $[0/\pm45/90]_s$ Laminate 66
5.12 Stress Distribution for $[\pm45/90]_s$ Laminate 67
5.13 Stress Distribution for $[0/45/0/45/0]_T$ Laminate 68

LIST OF TABLES

Table Page

3.1 Lamina Properties 15

3.2 Laminates Evaluated for Stress Concentrations 15

3.3 Required Inputs for the NASTRAN MAT8 Card 16

3.4 FEM Surface Boundaries 17

3.5 Mesh Seed Spacing per Model 18

3.6 Mesh Size per Surface 20

3.7 Numbering Scheme for Elements Around Cutout Boundary 22

3.8 Isotropic Plate Validation Results 25

4.1 Global X-Direction Stress Along Cutout Boundary $[0/\pm45/90]_s$ 38

4.2 Analytical SCF's for Isotropic Plate and Quasi-Isotropic Laminates 41

4.3 Analytical SCF's for Orthotropic Laminates 41

4.4 Analytical SCF's for Symmetric Anisotropic Laminates 42

4.5 Analytical SCF's for Unsymmetric Anisotropic Laminates 42

5.1 Symmetric Laminates – Analytical and Numerical SCF's for Circular Cutout 43

5.2 Unsymmetric Laminates – Analytical and Numerical SCF's for Circular Cutout 44

5.3 Laminate SCF – Circular – Symmetric Laminates 45

5.4 Laminate SCF – Circular – Unsymmetric Laminates 45

5.5 Laminate SCF – Square (R=0.4") – Symmetric Laminates 46

5.6 Laminate SCF – Square (R=0.4") – Unsymmetric Laminates 46

5.7 Laminate SCF – Square (R=0.3") – Symmetric Laminates 47

5.8 Laminate SCF – Square (R=0.3") – Unsymmetric Laminates 47

5.9 Laminate SCF – Square (R=0.2") – Symmetric Laminates 48

5.10 Laminate SCF – Square (R=0.2”) – Unsymmetric Laminates 48
5.11 Laminate SCF – Square (R=0.1”) – Symmetric Laminates 49
5.12 Laminate SCF – Square (R=0.1”) – Unsymmetric Laminates 49
5.13 Lamina SCF – Circular – Symmetric Laminates 56
5.14 Lamina SCF – Circular – Unsymmetric Laminates 56
5.15 Lamina SCF – Square (R=0.4”) – Symmetric Laminates 57
5.16 Lamina SCF – Square (R=0.4”) – Unsymmetric Laminates 57
5.17 Lamina SCF – Square (R=0.3”) – Symmetric Laminates 58
5.18 Lamina SCF – Square (R=0.3”) – Unsymmetric Laminates 58
5.19 Lamina SCF – Square (R=0.2”) – Symmetric Laminates 59
5.20 Lamina SCF – Square (R=0.2”) – Unsymmetric Laminates 59
5.21 Lamina SCF – Square (R=0.1”) – Symmetric Laminates 60
5.22 Lamina SCF – Square (R=0.1”) – Unsymmetric Laminates 60

NOMENCLATURE

Abbreviation	Definition
FEM	Finite Element Model
FEA	Finite Element Analysis
SCF	Stress Concentration Factor
SSF	Stress Severity Factor
SRF	Strength Reduction Factor
FWC	Finite Width Correction
BDF	Bulk Data File
F06	Analysis results text file
XDB	Analysis results PATRAN input file
UL	Upper Left (in reference to cutout corner)
UR	Upper Right (in reference to cutout corner)
LL	Lower Left (in reference to cutout corner)
LR	Lower Right (in reference to cutout corner)

CHAPTER 1

INTRODUCTION

1.1 Composite Overview

Composite materials are an ever evolving engineering feat that embodies the old adage “necessity is the mother of invention”. Monolithic structures have served their purpose throughout time as simple, cost-effective and easily repeatable but all structures can be altered to be made more efficient and more capable. Even the earliest civilizations saw the benefits of adding straw to clay bricks for added reinforcement. In modern times this same concept is employed in our roads and buildings using concrete reinforced with steel bars to significantly improve the strength and lifespan.

1.1.1 Historical Uses

The aerospace industry is unique by the standard that never before in history has it been necessary to defy gravity for a sustained period of time. Therefore the weight is the most critical property of any given structure on an aircraft. Metallics, woods and even ceramics can be sized to meet any static strength or fatigue requirement but the end goal is to be as efficient as possible. The advancement of fiber-reinforced polymers over the last century has continuously redefined the capabilities of aircraft and spacecraft.

The advent of plastics in the early twentieth century allowed scientists and engineers the opportunity to begin mixing the strongest materials used for structure with the lightest and cheapest materials used for everyday items. For several more decades, the focus of material development still centered around just understanding the basic principles of simpler isotropic materials such as elasticity, strength, stability and crack growth.

The 1940's brought about the first fiberglass boat and other composites began to replace small structural items on several developmental aircraft. While the lack of understanding and experience with composite materials caused hesitation in the aerospace industry, materials such as fiber glass were rapidly becoming main stream in other industries. The 1950's exploded with sports cars employing fiberglass bodies. Toward the end of the decade fiberglass would be used on the Boeing 707.

The 1960's led to a revolution of composite materials. The research community made composite material advancement a priority and the aerospace industry began to push the boundaries of the current materials. The Lockheed Martin SR-71 Blackbird was the single greatest advancement of an aircraft over the current technology. The SR-71 achieved speeds above Mach 3.3, which resulted in the skins reaching temperatures above 1000° due to the skin friction with the air. This required materials other than aluminum, which was the normal material used for aircraft skins. Titanium was the primary material used for the SR-71 but it's estimated that 15% of the aircraft was made of composites, primarily wing tips and skins (2009).

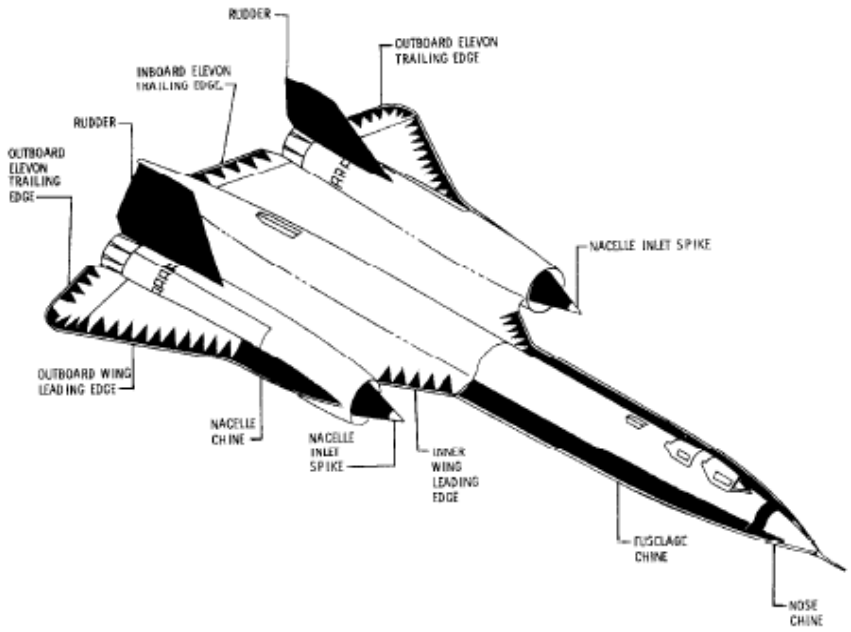

Figure 1.1 SR-71 Use of Composite Materials (Lockheed Martin, Courtesy of P.W. Merlin, 2009)

As the decades went on, composites became more and more common as primary structure on fighter jets, bombers, airliners and spacecraft. Just as Boeing was one of the first aviation companies to employ composites, they continue to lead the development and advancement of composites. The Boeing 777 made strides forward by using various types of composites for floor beams, landing gear bay doors and all control surfaces. In 2005 Boeing, and their various partners, began manufacturing the 787, which is over 50% composite. The aircraft fuselage was divided up into several sections and then each section was created to be a single piece of continuous skin with co-cured stringers, as can be seen below.

Figure 1.2 Boeing 787 Developmental Fuselage Section (Courtesy of Boeing.com)

As can be seen in Figure 1.2, cutouts are a common occurrence on an aircraft and present challenging scenarios to reduce the stress concentration. The research presented intends to show some unique solutions to reduce the stress at the corners.

1.1.2 Composite Materials

A composite is any combination of two or more unique materials. The composites that will be discussed in this paper are known as fiber-reinforced composites. This means that there is a collection of higher strength fibers located within a matrix. The bonding of these materials to each other to create a lamina is what provides the benefit over just using one material or the other on its own. A fiber strand may be incredibly stiff along its axial direction but alone it has no stability in its transverse direction. When these materials are bonded together the result is a high strength material along the axial direction of the fiber and a structurally capable material along the transverse direction.

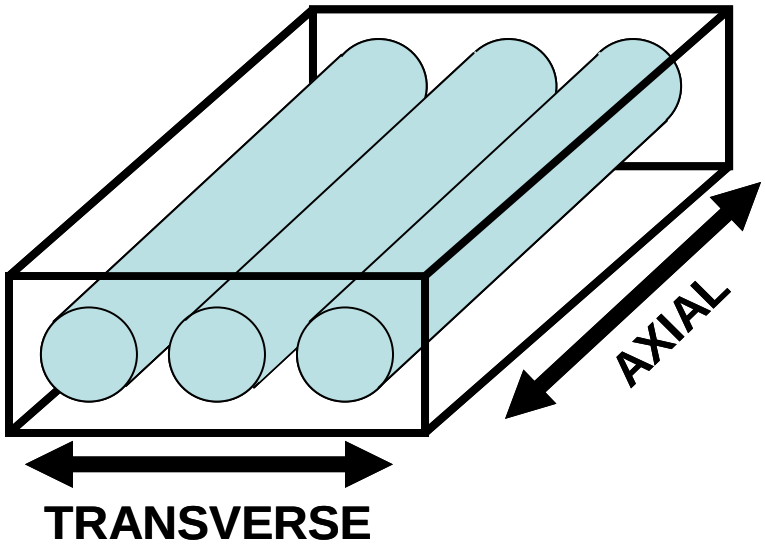

Figure 1.3 Continuous Fiber-Reinforced Lamina Definition

There are numerous types of fiber-reinforced composites, such as particulate, discontinuous, randomly oriented discontinuous and fabric. As these are not commonly used for aircraft structure, they will not be covered. While fiberglass composites are still common in aircraft, they are primarily used as protective barriers to prevent impact damage or moisture ingression from occurring on the higher strength composites.

Fiber-reinforced composites can be supported by several different matrix options, such as polymer, metal, ceramic or carbon. As stated earlier, the development of polymers in the twentieth century have led to composites reaching never before seen capabilities. Polymers are the most common matrix and allow for the greatest variety out of what the intent of the matrix should be. The typical polymers are either of the thermoset variety or the thermoplastic. The epoxy matrix will be evaluated in this paper, which is a thermoset polymer.

There are also several options of which fiber used to reinforce the composite, such as glass, carbon, aramid and boron. Aramid is more commonly known as Kevlar, which is typically used for bullet-proof vests. While it is very damage tolerant, it has relatively low compression strength and is therefore not typically used for aircraft. Boron is not very common with a polymer matrix. It is typically used with a metal matrix for situations at higher temperatures. Glass fibers, such as fiberglass, do not have the same stiffness capabilities that carbon fibers have and have therefore been reduced to more of a supporting role in association with carbon based laminates. The carbon fiber with an epoxy matrix is the most capable due to its high specific strength and high specific stiffness capabilities.

A common misnomer of carbon/epoxy composites is that when used in service they are much lighter than the nearest equivalent metallic. In all actuality, current design guidelines prevent the most efficient use of composites because of the lack of understanding at failure. There is not a universally accepted failure analysis criterion for composite laminates due to the inconsistent results between the analytical data and the test data. The most widely accepted failure criterion is actual test data for each material laminate being considered. The composites are tested to failure for various scenarios such as open-hole compression, open-hole tension, filled-hole compression, filled-hole tension and compression after impact, to name a few. There is also a wide array of tests for damage, fatigue, voids in the laminate and several other situations. The lack of physical understanding of composites is still an obstacle that prevents

using them to their utmost potential. The research presented in this document intends to show that patterns emerge from loading scenarios and the resultant stresses.

1.1.3 Laminate Properties

A material property and a laminate property are not necessarily continuous. A carbon/epoxy lamina is assumed to be symmetric in at least one plane, which is defined by the thickness. An isotropic property has an infinite number of planes of symmetry. An orthotropic plate has three mutually perpendicular planes of symmetry. An anisotropic plate has no planes of symmetry.

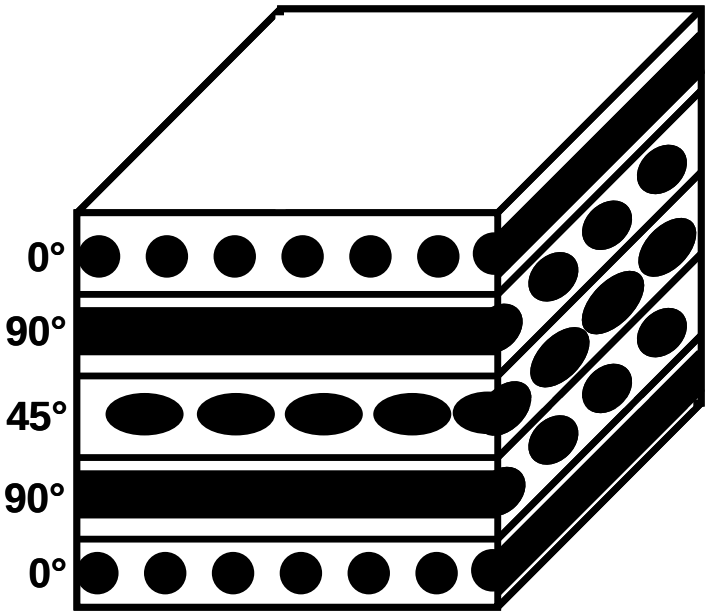

Figure 1.4 Laminate Stack-Up Definition

1.2 Cutouts

Carbon/epoxy composites provide the opportunity to eliminate inefficiencies such as strength and/or stiffness in unnecessary locations and/or directions. Composites also offer the unique opportunity of varying the laminate properties throughout different segments of the structure. Previously, to achieve an efficient structural assembly, different materials would be employed for different load paths and then those separate elements would have to be attached together in some form of a joint. Since the composite laminate can be designed specifically for each segment of a structural assembly, the composite can smoothly blend from one element to the next without an actual joint. The best example of this is co-cured skin and stringer elements. Integrally stiffened metallic panels exist but there are machining and forming limitations that prevent them from reaching true optimization.

Some inefficiency in an aircraft cannot be avoided, such as cutouts for access holes, panels, doors, penetrations and more. The only way to minimize the inefficiency is to design the laminate to redirect the load and avoid a potentially devastating stress concentration (SCF). In metallic structure the primary method to adjust the load distribution for a cutout is to increase the radius at the corner, which in turn decreases the SCF. Generally, this approach works until a cutout becomes a circle, at which point the SCF plateaus at a value of approximately 3.0. This method is still employed for composites, but the option to vary the laminate stack-up and redirect the load by altering material properties also exists. A circular cutout in a homogeneous material, as previously mentioned, is optimal at a SCF of 3.0 but a composite laminate may potentially achieve a value much less for a specific layup. It is very important to understand that adjusting the properties of the laminate to reduce the SCF may compromise other properties that will define its capability. A laminate consisting entirely of 0° plies will have a considerably large stiffness in the 0° direction. If a hole exists at the center of the laminate, a large SCF will occur, which can be minimized by adding ±45° plies. However, replacing a single 0° ply, or just adding a 45° ply to the stack-up, will significantly reduce the stiffness in the 0° direction.

1.3 Thesis Overview

1.3.1 Thesis Objectives

The objective of the research is to discover a correlation between the stresses in orthotropic, symmetric anisotropic and unsymmetric anisotropic laminates.

1.3.2 Chapter Layout

Chapter 2 will present the literature review over all of the topics covered by the research. It begins with stress concentration analysis in metallics from closed-form solutions. It will also cover the early research on measuring and calculating stress concentrations in composites from experimental data and analytical solutions.

Chapter 3 will present the finite element model generation and validation methodology. This will cover the plate sizing, meshing density, boundary conditions, properties and the validation with the closed-form isotropic solution. The process to obtain and report the data will also be explained, including the tools that were necessary.

Chapter 4 will present a review of composite macromechanics and classical lamination theory. It will also include an explanation of the closed-form solution for isotropic materials provided by Timoshenko and the closed-form solution for anisotropic materials provided by Lekhnitskii. Then using these solutions, the expected results for the quasi-isotropic, orthotropic and anisotropic laminates will be presented for each cutout.

Chapter 5 will present the results of the finite element analysis. These results will show the net effects of stacking sequencing at a stress concentration. The results will also show the overall effect that an unbalanced or unsymmetric laminate presents on a stress concentration. All orthotropic and anisotropic results will be compared to the closed-form solutions and assumptions about extrapolating the unsymmetric data will be provided.

Chapter 6 will present the conclusion and the explanation of any future efforts.

CHAPTER 2

LITERATURE REVIEW

2.1 Stress Concentrations in Metallics

SCF's have been known to exist in plate-like structure for over a century in various forms of cutouts, notches and cracks. Inglis (1913), a fellow at King's College in Cambridge, England, was the first to develop a theoretical solution to measure stress concentrations located at the boundary of an ellipse. He varied the sizes of the ellipses to cover shapes from a circle to an extremely narrow ellipse that could be assumed to represent a crack. He postulated that a rectangle could be defined by two ellipses intersecting obliquely. While he made mention of some error in this method, it was assumed to be quite small.

Heller et al (1958) made mention of Inglis' findings and proved that an ellipse could not accurately represent a rectangle. Heller was able to derive a mapping function that could accurately represent the stresses around a rectangular cutout with rounded corners.

Sobey (1963) developed his own mapping functions to analyze a rectangular cutout in an isotropic plate. He determined the stress concentrations at the corners for several loading conditions.

2.2 Stress Concentrations in Composites

Lekhnitksii (1968) derived the theory to analyze general anisotropic plates of infinite size with elliptical cutouts of various sizes. Lekhnitskii's formalism has primarily been used for

orthotropic plates due to the mathematical simplification when the plate has three mutually perpendicular planes of symmetry.

Daniel et al (1974) evaluated the effects that the material and stacking sequence would have in the presence of a hole in a finite width laminate plate. The paper covered strain distribution to failure, tensile and compressive SCF's and strength reduction factors (SRF) for multiple materials. Ten different laminate stacking sequences were considered, some of which were iterated for multiple materials. All of the laminates were either quasi-isotropic or orthotropic. Analytically, the plates were evaluated using Lekhnitskii's closed form solution for an infinite plate and the finite element method was used to represent the more realistic finite plate. The graphite/epoxy laminate resulted in the highest SCF and also suffered from the greatest SRF. The boron/epoxy laminates showed non-linear results at the boundary edges of the cutout but the graphite/epoxy laminate always remained linear. However the SCF's were calculated while all laminates were still in the linear elastic range. Both the boron/epoxy and the glass/epoxy laminates failed due to interlaminar effects but the graphite/epoxy laminate consistently failed in the plane perpendicular to the loading direction. The overall results showed that when the free boundary contained a relatively high SCF, the effects of the stacking sequence were greatly accentuated.

Whitney and Nuismer (1974) developed two separate criteria based on stress distribution to predict the uniaxial tensile strength of a laminate containing a cutout. The first approach assumed that failure would occur when the stress level at a point, measured some distance (d_0) from the edge of the cutout, reached the ultimate tensile strength of the unnotched laminate. The distance (d_0) was intended to represent the length from the edge of the cutout to the critical stress required to find a sufficient flaw capable of initiating failure. Theoretical and experimental results showed a reasonable correlation for a (d_0) value of 0.04 inches in glass/epoxy laminates. The second criterion assumed that failure could be predicted when an average stress of an area, measured some distance (a_0) from the edge of the cutout, reached

the unnotched tensile strength of the laminate. It was assumed that using an average stress over a large area would allow the laminate some capability to redistribute the local stress concentration. Theoretical and experimental results showed a reasonable correlation for an (a_0) value of 0.15 inches. The average stress method (a_0) provided better correlation than the point stress method (d_0). Both methods were intended to prove that the measurements were a material property that was independent of both the laminate stack-up and the local stress distribution but this was later proved to be false.

Konish and Whitney (1975) derived an approximate solution to determine the normal stress distribution adjacent to a circular hole in an infinite orthotropic laminate based on several of the laminate compliance stiffnesses. They believed a simple relationship existed between the isotropic solution and an orthotropic solution. The difference between a homogenous material and a laminate is that metallics are continuous along the boundaries but laminates have a perforated edge composed of fibers and matrix. This requires that a larger area be used to determine the SCF in the composite. The exact isotropic polynomial solution was modified to include sixth and eighth order terms to better represent an orthotropic material. Another solution was derived by simply scaling the isotropic solution by the ratio of the isotropic SCF to the orthotropic SCF. Both solutions were compared to the exact orthotropic solution from Lekhnitskii. The extended isotropic solution showed a much better correlation for various laminate stack-ups than did the scaled isotropic solution.

Rajaiah (1983) applied the previously developed mapping theory with Lekhnitskii's theory to evaluate the SCF's for several rectangular shapes. His intentions were to provide results directly to engineers to be used in the industry. He found that cutout optimization for orthotropic plates resulted in a greater decrease of the SCF than in isotropic plates.

Ko (1985) analyzed the stress concentrations at the perimeter of a cutout in various graphite/epoxy laminates. He used Lekhnitskii's anisotropic plate theory to calculate the SCF of a graphite/epoxy lamina. Ko calculated the laminate properties by using a mixture rule and he

never specifically stated the stack-up orientation of the laminate but he did mention that it was anisotropic. He varied the fiber orientation relative to the loading direction to quantify the effects of an unbalanced laminate. Using the Point Stress Criterion and the Average Stress Criterion developed by Whitney and Nuismer (1974), Ko was able to determine the hole size effects on the lamina. He discovered that the hole size effect became significant when the diameter of the hole was less than 1.2 inches. He also found that for a 0.125 inch diameter hole, a (d_0) value of 0.05 inches and an (a_0) value of 0.15 inches showed good correlation with the measured SCF values.

Tan (1988) developed a series of finite-width correction (FWC) factors for both orthotropic and anisotropic plates with an elliptical cutout. He focused the paper on the adjustment of SCF's for the plate sizing and he also presented how test data of a finite plate could be extrapolated to an infinite width plate. The use of an isotropic FWC factor can lead to a significant amount of error since it has no relation to the material properties, whereas an anisotropic FWC factor is dependent upon the material properties and the SCF as determined by Lekhnitskii's theory. Tan derived the FWC factors for orthotropic and anisotropic plates by two different methods. The first method was to determine the exact 2D anisotropic stress distribution from Lekhnitskii's theory and use a ratio of the SCF for the infinite plate to the finite plate for the FWC factor. The second method was to assume an approximate orthotropic SCF for the infinite plate which greatly reduces the necessary calculations. A magnification factor based only on the ratio of the width of the cutout to the width of the plate was added to the approximate orthotropic solution for an increased percentage of accuracy.

Rezaeepazhand and Darbari (2005) derived the mapping formulas to be used with Lekhnitskii's theory for rectangular, triangular and hexagonal cutouts. Finite element models were created to validate their results, and they achieved good correlation. They were able to show that increasing the fiber angle at the cutout decreased the SCF.

Rezaeepazhand and Jafari (2010) expanded on the (2005) article and used the mapping function to run the analysis for several quasi-rectangular cutouts of various sizes and various corner radii. For each cutout a maximum and minimum SCF was determined and the fiber orientation and cutout orientation were rotated to optimize to the loading condition. The general result was that either the cutout orientation at an angle of 45° or the fiber orientation at an angle of 45° had the lowest SCF.

CHAPTER 3

FINITE ELEMENT MODEL GENERATION AND VALIDATION

This chapter explains the procedures used to create the model and the methodology used to validate the results. MSC PATRAN was used for the pre and post-processing and MSC NASTRAN was used for the analysis.

3.1 Geometry and Material

3.1.1 Plate Configurations

The research required the use of five separate models, each consisting of a different cutout. The general model configuration can be seen in Figure 3.1. The overall plate dimensions for each model are 60.0 inches long (a) by 30.0 inches wide (b). All cutouts have a width (w) of 2.0 inches but each with different radii (r) at the corners. The radii for the models are 0.1 inches, 0.2 inches, 0.3 inches, 0.4 inches and 1.0 inch, which becomes a circle.

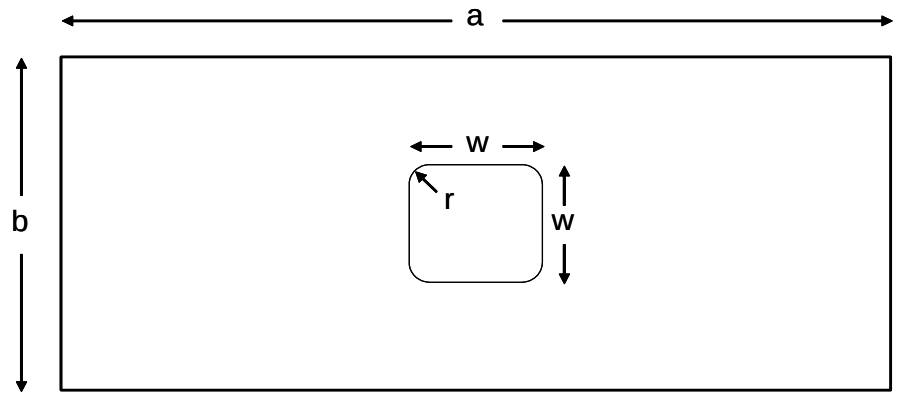

Figure 3.1: Plate Dimensions

3.1.2 Lamina and Laminate Properties

The material used for this study is a carbon/epoxy unidirectional fiber-reinforced lamina, typical of what is used for aircraft structure. Table 3.1 defines the properties used for this study.

Table 3.1 Lamina Properties

Carbon/Epoxy Lamina Properties	
E_1	21.3 Msi
E_2	1.5 Msi
E_3	1.5 Msi
G_{12}	1.0 Msi
G_{13}	1.0 Msi
G_{23}	0.54 Msi
v_{12}	0.27
v_{13}	0.27
v_{23}	0.54
t	0.01 in

Laminates of all categories were evaluated in an attempt to draw trends from balanced to unbalanced and symmetric to unsymmetric. The following is a table of all of the laminates evaluated for this study.

Table 3.2 Laminates Evaluated for Stress Concentrations

Quasi-Isotropic	Orthotropic (Balanced & Symmetric)	Anisotropic – Symmetric (Unbalanced)	Anisotropic - Unsymmetric	
$[0/\pm45/90]_S$	$[0/\pm45/0]_S$	$[45/0]_S$	$[0/45/90]_T$	$[0/\pm45/0]_T$
$[45/0/90/-45]_S$	$[\pm45/0]_S$	$[45/0/90]_S$	$[0/45/90]_{2T}$	$[0/45/0/-45/0]_T$
	$[\pm45/90]_S$	$[45/0/\overline{90}]_S$	$[0/\pm45/90]_T$	$[45_2/0/-45_2]_T$
	$[0/\pm45/\overline{0}]_S$	$[0/45/90]_S$	$[0/\pm45/90]_{2T}$	$[45_2/0_2/-45_2]_T$
	$[45/0/-45/0]_S$	$[0/45/\overline{0}]_S$	$[45/0]_{2T}$	$[\pm45/0]_T$
			$[45/0/-45/0]_T$	$[45/0/90/-45]_T$
			$[45/0_2/-45]_T$	$[0/\pm45/0/\pm45/0]_T$
			$[45/0/90/0/-45]_T$	$[0_2/45_2/90_2]_T$

3.2 Model Generation

3.2.1 NASTRAN Properties

A MAT8 card is used in NASTRAN to define the material properties of a single lamina. Table 3.3 shows the necessary inputs for the MAT8 card. The density input was left blank because weight is not a concern of this study.

Table 3.3 Required Inputs for the NASTRAN MAT8 Card

NASTRAN MAT8 Card Inputs
E_1
E_2
v_{12}
G_{12}
G_{13}
G_{23}
ρ

A PCOMPG card is used in NASTRAN to define the laminate stack-up. It was selected by default from the Laminate Tool in PATRAN. For the uses of this study there are no differences between the PCOMP and the PCOMPG cards. A sample PCOMPG card is displayed in Figure 3.2 for a laminate composed of $[0/\pm45/90]_s$.

Col 1	Col 2	Col3	Col 4	Col 5	Col 6	Col7	Col 8
PCOMPG	2					0.	0.
	1	1	0.01	0.	YES		
	2	1	0.01	45.	YES		
	3	1	0.01	-45.	YES		
	4	1	0.01	90.	YES		
	5	1	0.01	90.	YES		
	6	1	0.01	-45.	YES		
	7	1	0.01	45.	YES		
	8	1	0.01	0.	YES		

Figure 3.2 Sample PCOMPG Card of $[0/\pm45/90]_s$

The first row of the PCOMPG card defines the property ID in column 2 and the reference temperature and damping coefficient in columns 7 and 8, respectively. Each successive row after the first defines an individual ply. Column 2 states the ply number in the stack-up and column 3 references the applicable MAT8 card. Column 4 defines the ply thickness and column 5 defines the angle of the ply relative to the material axis of the element. The material axis is defined within the element to equal the global coordinate system (Coord 0). Column 6 commands NASTRAN to output the individual stresses for each ply.

3.2.2 Meshing

The meshing of the model is critical for two main reasons. One, the model must be optimized to create a stress distribution without influence from model abnormalities, which will in turn provide the most accurate results. Two, the mesh must be organized so that the desired data can be collected from the massive volume of data produced by each iteration of numerical analysis.

The plate was divided up into multiple surfaces, which need to be meshed individually. These are trimmed surfaces since it is not necessary to have a parametric surface or isometric elements for this study. The surfaces become increasingly larger in area as the distance grows from the cutout to allow for larger elements. All of the models were formatted to have common geometry except for the corner radii of the cutout. Table 3.4 reports the common surface dimensions for each plate and Figure 3.3 displays the corresponding surfaces.

Table 3.4 FEM Surface Boundaries

	Surface Border Distance From Plate Center (in)					
Surface	Cutout	1	2	3	4	5 & 6
Horizontal	1.0	1.5	2.5	5.0	15.0	30.0
Vertical	1.0	1.5	2.5	5.0	15.0	15.0
Outer Radius	r	0.5 + r	1.0 + r	2.5 + r	N/A	N/A

*r refers to cutout corner radius for respective plate

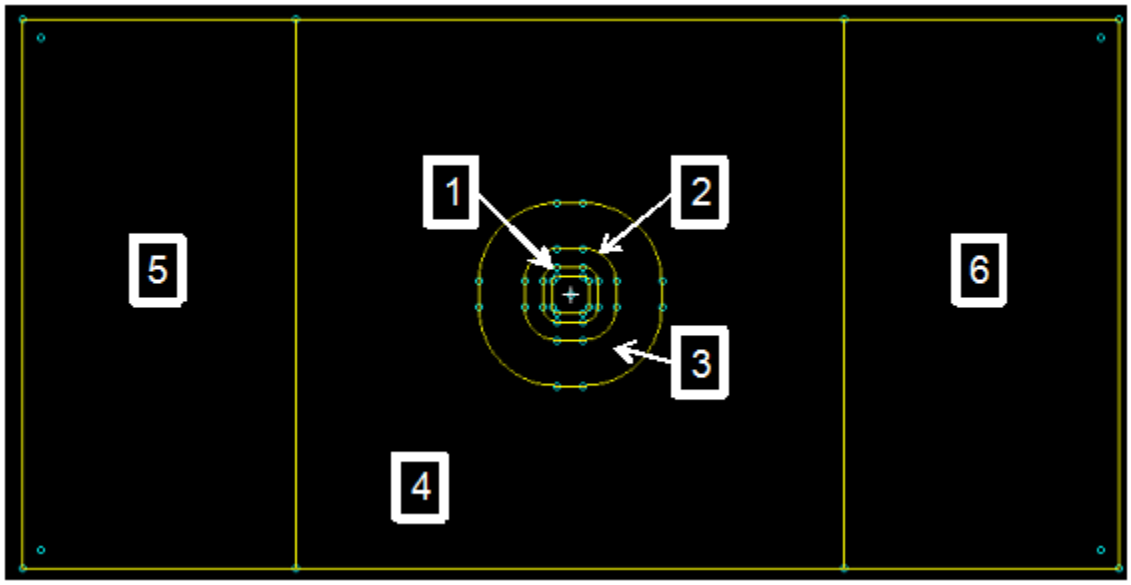

Figure 3.3 FEM Surfaces of Plate with Square Cutout (r=0.3")

The size of the elements is controlled by mesh seeding for Surface 1, which is closest to the cutout boundary. The mesh seed measurements are explained in Table 3.5 and an example is shown in Figure 3.4. The mesh seeding that follows the contour of the corner is constant. The mesh seeding that spans the flat edges of the cutout uses a two-way bias. This means that it has a beginning value at one end of the curve and expands to the maximum value at the midspan and then reduces back to the original value at the opposite end.

Table 3.5 Mesh Seed Spacing per Model

	Corner Radius (in)	Mesh Seed Spacing (in)		
		Corner (constant)	Side (two-way bias)	
			minimum	maximum
Model 1	0.1	0.008	0.008	0.048
Model 2	0.2	0.01	0.01	0.05
Model 3	0.3	0.01	0.01	0.05
Model 4	0.4	0.01	0.01	0.03
Model 5	1.0	0.01	N/A	N/A

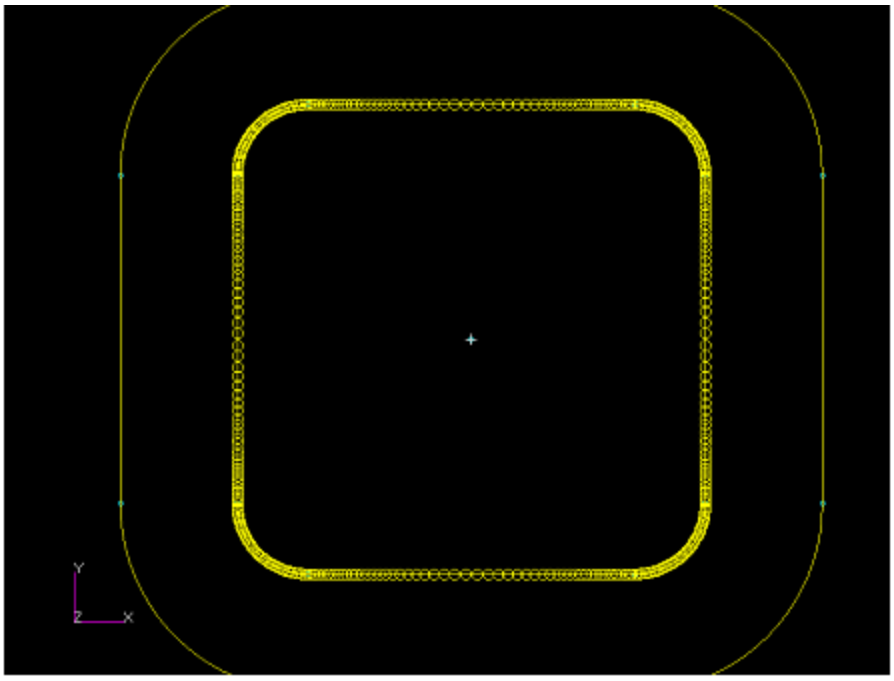

(a)

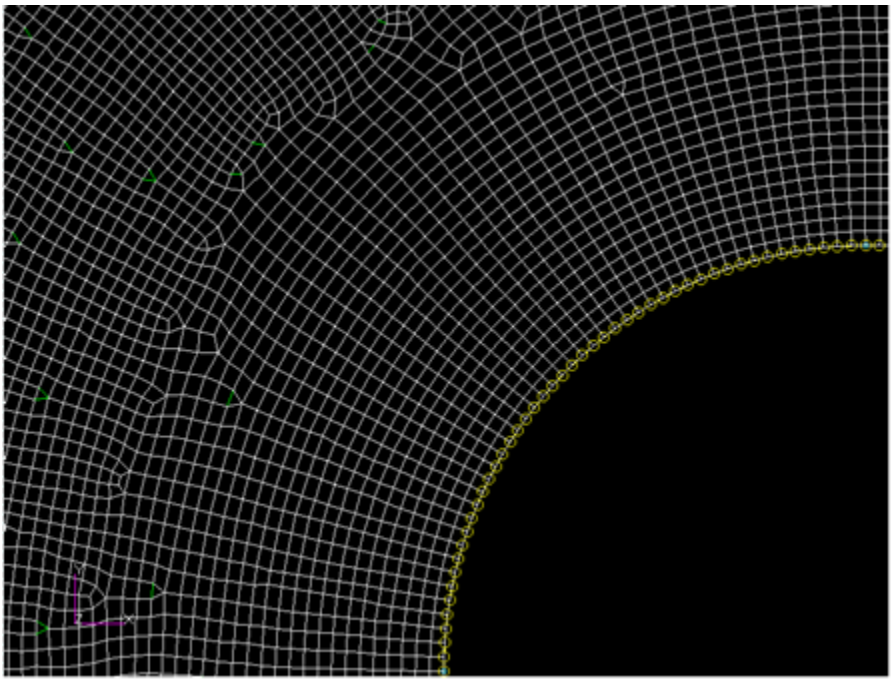

(b)

Figure 3.4 (a) Mesh Seeding for Model 3 (b) Mesh Seeding for Corner of Model 3 with Mesh

The element sizing is defined by the mesh seeding along the cutout boundary and by the proposed value within the auto-mesher for the perpendicular distance relative to the cutout boundary. The “Hyper Paver” auto-meshing function within Patran was used to create the mesh for each surface. The mesh sizing set by the auto-meshing function can be seen in Table 3.6.

Table 3.6 Mesh Size per Surface

	Surface Border Distance From Plate Center (in)				
Surface	1	2	3	4	5 & 6
Mesh Size (in)	0.01	0.05	0.2	0.5	0.5

A completely meshed model can be seen in Figure 3.5. The mesh is very noticeably dense near the cutout and expands a great deal as the distance grows from the cutout edges. The model could be made to be coarser in the outlying surfaces but considering the computational power available, this was not necessary. All elements near cutout corners and within the first six rows were verified to be CQUAD elements to avoid any unnecessary stiffness in the region of the peak stresses, as can be seen in Figure 3.4(b).

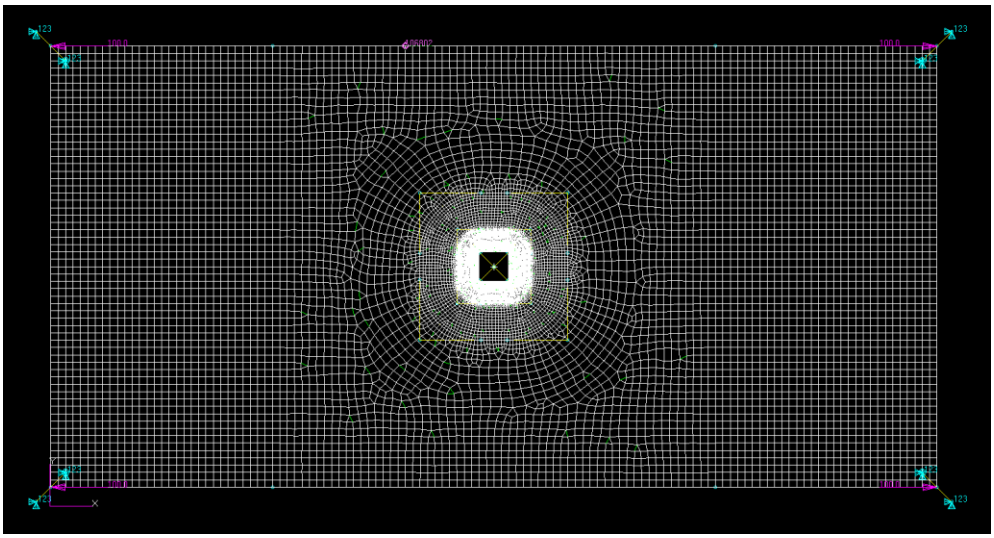

Figure 3.5 Plate Model with Mesh for Square Cutout

3.2.3 Boundary Conditions and Applied Loads

The boundary conditions on a model must be applied very precisely and with clear intent. An under-constrained model may fail to execute and an over-constrained model may report skewed results.

All of the models in this study employ CBUSH elements at the corners to restrain the model from rigid-body-motion. Each CBUSH is defined with relatively low stiffness values of 100 lbs/in in the translational directions, so as to not allow any influence on the loads beyond simple round-off. A pair of CBUSH's is located at each corner of the model with one end of each CBUSH attached to a node embedded in the plate away from the edge and another node offset from the plate. The offset node has a single-point constraint applied that prevents translation in any direction. One CBUSH is used to slightly restrain the plate from any in-plane translation and the other CBUSH is used to restrain the plate from any out-of-plane translation.

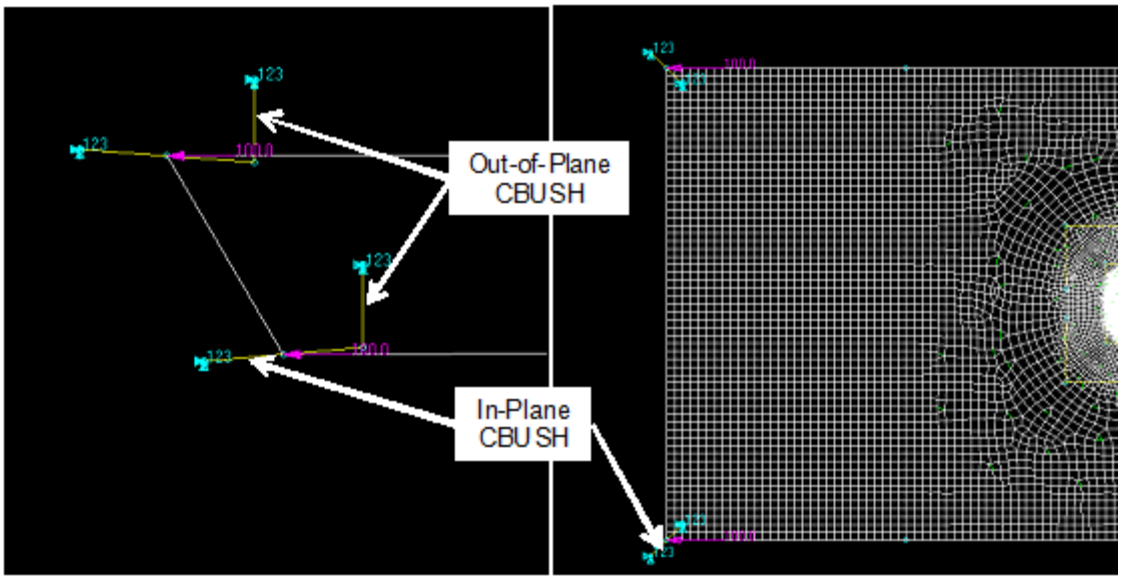

Figure 3.6 CBUSH Elements and Distributed Loads

A distributed load of 100 lbs/in is applied to each vertical end of the plate. The distributed load is useful due to its simplified loading based solely on the length of the edge.

3.2.4 Numbering Scheme

Due to the massive amounts of data that result from FEA, a degree of organization is necessary to ensure that the data that is processed is the data that is desired and also to allow for proofs along the way. A numbering scheme was developed for the following reasons:

1. Collect element stresses from around the cutout for SCF comparison
2. Collect CBUSH loads to ensure a balanced model
3. Collect displacements to quantify out-of-plane bending
4. To process the aforementioned items with an automated program

The elements and nodes mentioned above were the only items that needed to be collected from the FEA and so therefore all other elements and nodes were renumbered to an offset value well above the maximum identification value in the numbering scheme.

The numbering scheme of the elements where the SCF data is gathered is divided up by corners. Each corner is then divided by rows according to the distance offset from the edge of the cutout. The numbering scheme is explained in Table 3.7 and the pattern in which the elements were numbered for each corner is shown in Figure 3.7. Only as many elements that could fit within the numbering scheme were selected. The results were proofed to be certain that the peak stress never occurred near the edge of the selected elements.

Table 3.7 Numbering Scheme for Elements Around Cutout Boundary

	Row 1	Row 2	Row 3	Row 4	Row 5	Row 6
Offset (in)	0.005	0.015	0.025	0.035	0.045	0.055
Upper Left	1001-1099	1101-1199	1201-1299	1301-1399	1401-1499	1501-1599
Upper Right	2001-2099	2101-2199	2201-2299	2301-2399	2401-2499	2501-2599
Lower Left	3001-3099	3101-3199	3201-3299	3301-3399	3401-3499	3501-3599
Lower Right	4001-4099	4101-4199	4201-4299	4301-4399	4401-4499	4501-4599

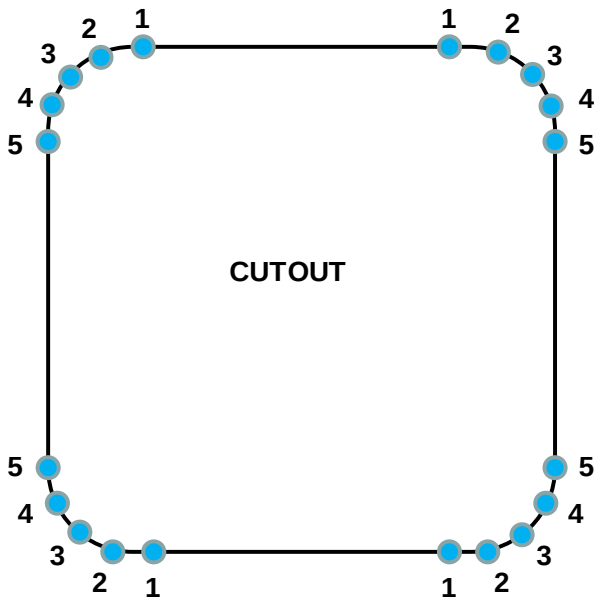

Figure 3.7 Corner Elements Numbering Order (See Table 3.7)

Eight nodes were collected to monitor the displacement of the plate in various locations. The number scheme of these nodes is shown in Figure 3.8. The CBUSH elements were also numbered in a similar manner.

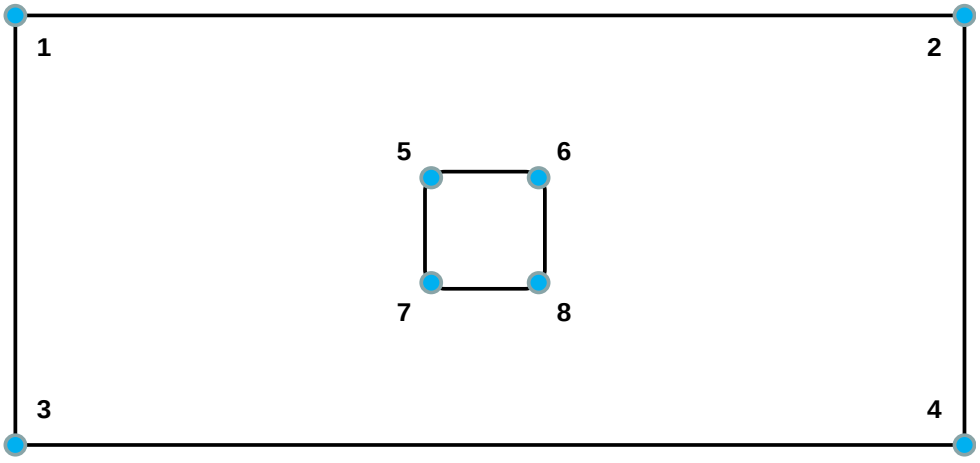

Figure 3.8 Displacement Node Numbering Order

3.3 Obtaining Results

3.3.1 Controlled Output

The numbering scheme explained in the previous sub-section was constructed to make outputting and processing the data possible. Commands have been placed in the Bulk Data File (BDF), which is the NASTRAN input file, to output the results of the stresses in the elements referenced in Table 3.7, the displacements of the previously referenced nodes and the stresses in the CBUSH elements. The results were populated into an F06 file for each laminate analyzed for each model. The F06 files are the NASTRAN results in text form.

A shell element defined with a PCOMPG card in NASTRAN outputs the stresses according to the property orientation angle. Therefore the NORMAL-1, NORMAL-2 and SHEAR-12 results correspond to the axial fiber stress, the transverse stress and the in-plane shear stress, respectively.

3.3.2 Processing Data

A unix script was used to remove all information that did not reference any of the aforementioned element or node ID's. The remaining information was then read into unique spreadsheet tabs for each F06 file. A spreadsheet was created for each model to be populated by all of the corresponding F06 files.

Each spreadsheet then had internal macros that would data mine the bulleted items below for each corner at each respective offset.

- Individual ply stresses
- Average global x-direction stress of all plies through the thickness per element
- Average max principal stress of all plies through the thickness per element
- Displacements (only taken at edge and mid-point of curve)

3.4 Validation

Each model must be verified against known results prior to the beginning of the study. It must be proven that the model can return accurate results as intended by the operator. The following closed-form solutions will be presented to validate the model but they will be explained in greater detail in the following chapter, Chapter 4 - Analytical Results.

3.4.1 Isotropic Plate

Timoshenko developed a set of equations (Eq. 4.20) to evaluate the stresses in circular cutouts in infinitely wide isotropic plates, which will be explained in the following chapter, Chapter 4 Analytical Results. Sobey developed a set of equations (Eq. 4.23) to evaluate the SCF's in an infinitely wide plate with rectangular cutouts with rounded corners. These equations will also be explained in the following chapter.

Table 3.8 Isotropic Plate Validation Results

	Circular	Square			
Corner Radii (in)	1.0	0.4	0.3	0.2	0.1
Analytical SCF	3.00	3.13	3.38	3.79	4.50*
Numerical SCF	3.02	3.17	3.40	3.80	4.67
Error (%)	0.6%	1.3%	0.6%	0.3%	3.8%

*Geometry is on lower boundary of applicability and may be inaccurate

CHAPTER 4

ANALYTICAL RESULTS

Analytical results were used to validate the isotropic models and then predict the peak SCF's at the corners of each respective model. Currently a SCF can be obtained for the orthotropic and anisotropic plates using Lekhnitskii's formalism but the location cannot be predicted. The following analysis will show how to calculate the SCF's for each of the laminates from Lekhnitskii's closed-form solution and then the results will be compared to the numerical results in the following chapter.

4.1 Composites Analysis Review

4.1.1 Macromechanics

Overall, the stress and strain components of a composite lamina are defined by the generalized Hooke's law.

$$\sigma_{ij} = C_{ijkl}\varepsilon_{kl} \tag{4.1}$$

Where C_{ijkl} is a stiffness matrix of the material.

For an isotropic material, only two material properties are required to adequately define the stress-strain relationship. However for the complete definition of a composite lamina, thirty-six elastic constants are required. To reduce the analysis complexity, certain assumptions must be made.

- The carbon/epoxy lamina is orthotropic and transversely isotropic
- The lamina is thin, with its planar dimensions much larger than its thickness
- Only plane stress will be applied
- All displacements are relatively small compared to the thickness of the laminate

The last bullet-point is not always satisfied for an unsymmetric laminate but all discrepancies will be noted for observation. The numerical results of the laminates in question will still be compared to the analytical results.

For a plane stress condition ($\sigma_z = \tau_{yz} = \tau_{xz} = 0$), Eq. 4.1 can be rewritten as shown in Eq. 4.2. The unique elastic constants are E_1, E_2, G_{12} and v_{12}.

$$\begin{bmatrix} \sigma_1 \\ \sigma_2 \\ \tau_6 \end{bmatrix} = \begin{bmatrix} Q_{11} & Q_{12} & 0 \\ & Q_{22} & 0 \\ sym & & Q_{66} \end{bmatrix} \begin{bmatrix} \varepsilon_1 \\ \varepsilon_2 \\ \gamma_6 \end{bmatrix} \tag{4.2}$$

$$Q_{11} = \frac{E_1}{1 - \nu_{12}\nu_{21}} \tag{4.3}$$

$$Q_{22} = \frac{E_2}{1 - \nu_{12}\nu_{21}} \tag{4.4}$$

$$Q_{12} = \frac{\nu_{12}E_2}{1 - \nu_{12}\nu_{21}} \tag{4.5}$$

$$Q_{66} = G_{12} \tag{4.6}$$

$$\frac{\nu_{12}}{E_1} = \frac{\nu_{21}}{E_2} \tag{4.7}$$

If the lamina principal axes (1,2) do not coincide with the reference axes (x,y), then the lamina properties must be transformed to the equivalent values along the references axes. The transformation matrix [T] is applied as follows.

$$\begin{bmatrix} \sigma_1 \\ \sigma_2 \\ \tau_6 \end{bmatrix} = \left[T_\sigma(\theta)_\sigma\right] \begin{bmatrix} \sigma_x \\ \sigma_y \\ \tau_s \end{bmatrix} \quad \text{or} \quad \begin{bmatrix} \sigma_x \\ \sigma_y \\ \tau_s \end{bmatrix} = \left[T_\sigma(\theta)_\sigma\right]^{-1} \begin{bmatrix} \sigma_1 \\ \sigma_2 \\ \tau_6 \end{bmatrix} \tag{4.8}$$

$$\left[T_\sigma(\theta)_\sigma\right]=\begin{bmatrix} m^2 & n^2 & 2mn \\ n^2 & m^2 & -2mn \\ -mn & mn & m^2-n^2 \end{bmatrix} \tag{4.9}$$

$$\left[T_\sigma(-\theta)_\sigma\right]=\begin{bmatrix} m^2 & n^2 & -2mn \\ n^2 & m^2 & 2mn \\ mn & -mn & m^2-n^2 \end{bmatrix} \tag{4.10}$$

$$m=\cos(\theta) \tag{4.11}$$

$$n=\sin(\theta) \tag{4.12}$$

4.1.2 Classical Lamination Theory

The classical lamination theory (CLT) is used to explain the behavior of a laminate as it pertains to the stacking sequence and the properties of the individual layers. The CLT builds on the assumptions stated in regards to the lamina definition, as can be seen below.

- Displacements are continuous and linear throughout the laminate
- Lines perpendicular to the surface remain perpendicular after deformation
- Strain-displacement and stress-strain relationships remain linear

The following diagram explains the stress-strain relationship of the individual lamina throughout the thickness of the laminate. The lamina modulus is reduced according to the angle offset from the reference axes of the laminate.

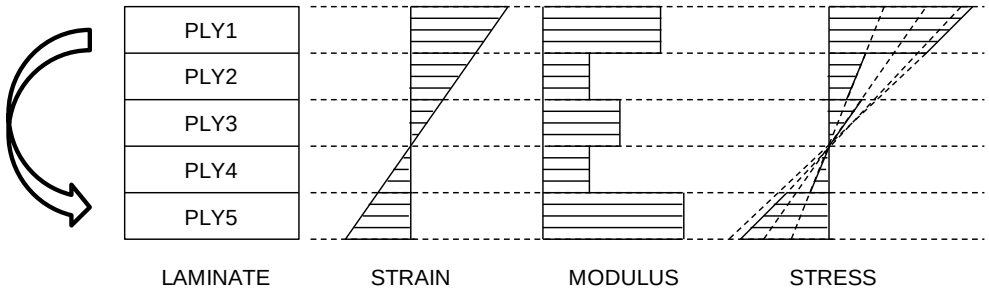

Figure 4.1 Stress-Strain Relation in a Laminate

To simplify the laminate analysis, CLT utilizes the relationship between the deformation of the laminate and the applied forces and moments. The strain is defined for any lamina, k, as shown in Eq. 4.13, where ε^0 is the laminate mid-plane strain and κ is the laminate curvature.

$$\begin{bmatrix} \varepsilon_x \\ \varepsilon_x \\ \gamma_s \end{bmatrix}_k = \begin{bmatrix} \varepsilon_x^0 \\ \varepsilon_y^0 \\ \gamma_s^0 \end{bmatrix} + z_k \begin{bmatrix} \kappa_x \\ \kappa_x \\ \kappa_s \end{bmatrix} \tag{4.13}$$

The lamina stresses are determined by Eq. 4.14 for a given strain and curvature.

$$\begin{bmatrix} \sigma_x \\ \sigma_x \\ \tau_s \end{bmatrix}_k = \begin{bmatrix} Q_{xx} & Q_{xy} & Q_{xs} \\ Q_{yx} & Q_{yy} & Q_{ys} \\ Q_{sx} & Q_{sy} & Q_{ss} \end{bmatrix}_k \begin{bmatrix} \varepsilon_x^0 \\ \varepsilon_y^0 \\ \gamma_s^0 \end{bmatrix} + z \begin{bmatrix} Q_{xx} & Q_{xy} & Q_{xs} \\ Q_{yx} & Q_{yy} & Q_{ys} \\ Q_{sx} & Q_{sy} & Q_{ss} \end{bmatrix}_k \begin{bmatrix} \kappa_x \\ \kappa_x \\ \kappa_s \end{bmatrix} \tag{4.14}$$

The lamina stresses are transformed into representative in-plane forces and moments per unit width based upon the location in the stack-up, as is shown in Eq. 4.15.

$$\begin{bmatrix} N_x \\ N_x \\ N_s \end{bmatrix} = \sum_{k=1}^{n} \int_{z_{k-1}}^{z_k} \begin{bmatrix} \sigma_x \\ \sigma_x \\ \tau_s \end{bmatrix}_k dz$$

$$\begin{bmatrix} M_x \\ M_x \\ M_s \end{bmatrix} = \sum_{k=1}^{n} \int_{z_{k-1}}^{z_k} \begin{bmatrix} \sigma_x \\ \sigma_x \\ \tau_s \end{bmatrix}_k z dz \tag{4.15}$$

The z_k and z_{k-1} values represent the upper and lower surfaces of lamina k, respectively.

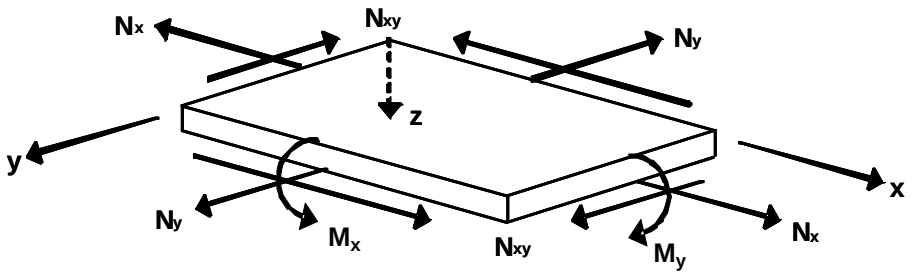

Figure 4.2 Element of Single Layer with Force and Moment Resultants

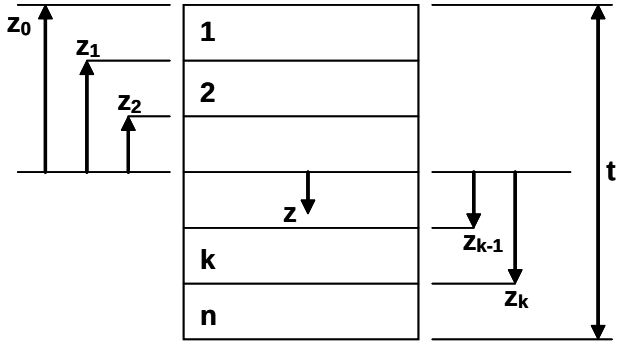

Figure 4.3 Laminate Plate Geometry and Numbering Scheme

The complete force-deformation and moment-deformation relationships are defined by Eq. 4.16 and Eq. 4.17.

$$\begin{bmatrix} N \\ M \end{bmatrix} = \begin{bmatrix} A & B \\ B & D \end{bmatrix} \begin{bmatrix} \varepsilon^0 \\ \kappa \end{bmatrix} \tag{4.16}$$

$$A_{ij} = \sum_{k=1}^{n} Q_{ij}^{k} (z_k - z_{k-1})$$

$$B_{ij} = \frac{1}{2} \sum_{k=1}^{n} Q_{ij}^{k} (z_k^2 - z_{k-1}^2) \tag{4.17}$$

$$D_{ij} = \frac{1}{3} \sum_{k=1}^{n} Q_{ij}^{k} (z_k^3 - z_{k-1}^3)$$

However it is much more common to use the inverse relationship of Eq. 4.16 since the applied loads and moments are typically provided and the stresses and strains need to be determined. b^T is the transpose of the b matrix.

$$\begin{bmatrix} \varepsilon^0 \\ \kappa \end{bmatrix} = \begin{bmatrix} a & b \\ b^T & d \end{bmatrix} \begin{bmatrix} N \\ M \end{bmatrix} \tag{4.18}$$

$$\begin{bmatrix} a & b \\ b^T & d \end{bmatrix} = \begin{bmatrix} A & B \\ B & D \end{bmatrix}^{-1} \tag{4.19}$$

4.2 Stress Concentrations

4.2.1 Isotropic Plate

It was necessary to establish and validate a baseline model of a circular cutout prior to the actual research. A homogeneous material property of approximately the same values as aluminum was used for the baseline analysis validation. However, the actual material properties for the isotropic plate are inconsequential since the closed-form solution reduces to only contain values based on the geometry of the plate, as can be seen below.

$$\begin{aligned}
\sigma_r &= \frac{1}{2}\sigma\left(1-\frac{a^2}{r^2}\right)+\frac{1}{2}\sigma\left(1-\frac{4a^2}{r^2}+\frac{3a^4}{r^4}\right)\cos 2\theta \\
\sigma_\theta &= \frac{1}{2}\sigma\left(1+\frac{a^2}{r^2}\right)-\frac{1}{2}\sigma\left(1+\frac{3a^4}{r^4}\right)\cos 2\theta \\
\tau_{r\theta} &= -\frac{1}{2}\sigma\left(1+\frac{2a^2}{r^2}-\frac{3a^4}{r^4}\right)\sin 2\theta
\end{aligned} \tag{4.20}$$

When the stress is taken along the cutout boundary, the equations reduce to that shown in (4.21). The equations further reduce when the peak stress concentration is realized at the top and bottom of the hole (θ=π/2 or 3 π/2), for a horizontal loading direction.

$$\begin{aligned}
&\sigma_r = 0 \\
&\sigma_\theta = \sigma\left(1-2\cos 2\theta\right) \\
&\tau_{r\theta} = 0
\end{aligned} \tag{4.21}$$

$$\sigma_{\theta=\pi/2} = 3\sigma$$

A hole loaded in uniaxial tension will achieve a stress concentration of 3.0, as shown above. The validation model showed excellent correlation with this, as explained in Section 3.4. The diameter of the hole was set to equal the width of the square cutout that would eventually be used in the analysis. This is essentially the same concept as the corner radii being increased until the adjacent corners meet in the center.

The intent of the model is to provide an accurate measurement of stress concentrations for a cutout in an infinite plate. Since it is not practical to model an infinite plate, a representative finite width plate must be determined. An attempt to model an infinite plate will provide diminishing returns as the plate grows in dimensions. Computer processors of today's capabilities will allow the analysis of a plate which is seemingly equivalent to an infinite plate but the accuracy gained is of little value added. The Heywood (1952) formula, taken from Peterson's *Stress Concentrations Factors* (2008) and displayed below, is used for preliminary sizing of the isotropic plate.

$$K_{tg} = \frac{2 + \left(1 - d / H\right)^3}{\left(1 - d / H\right)} \tag{4.22}$$

$$K_{tg} = \frac{2 + \left(1 - 2.0 / 30.0\right)^3}{\left(1 - 2.0 / 30.0\right)} = 3.014$$

For a plate height of 30.0 inches and hole diameter of 2.0 inches, a stress concentration of 3.014 results. When compared to Timoshenko's closed-form solution of a hole in an infinite plate, the resulting accuracy is within 0.5% error. This is considered to be an optimal size for the plate, and when compared to the validation results, shows near perfect correlation. The plate width was set by common modeling guidelines, which says the length of the plate in the direction of the applied load should be at least twice the length of the transverse direction. Therefore the width of the plate is set to be 60.0 inches.

Peterson's text (2008) provides a reference to the work performed by Sobey (1963) to determine the stress concentrations in an isotropic plate around rectangular cutouts with rounded corners. It is noted that a square opening with a corner radii of approximately one-third that of the width of the cutout has a lower stress concentration than that of a circular cutout.

Sobey presented an equation based on a series of factors and geometric parameters to calculate the stress concentration from a closed-form solution. For a square cutout, the equation is only valid for a range of ($0.05 \leq {}^{r}/_{2b} \leq 0.5$), where *r* represents the radius at the corner and *w* represents width of the cutout.

$$
\begin{aligned}
K_t &= C_1 + C_2\left({}^{b}/_{a}\right) + C_3\left({}^{b}/_{a}\right)^2 + C_4\left({}^{b}/_{a}\right)^3 \\
C_1 &= 14.815 - 22.308\sqrt{{}^{r}/_{2b}} + 16.298\left({}^{r}/_{2b}\right) \\
C_2 &= -11.201 - 13.789\sqrt{{}^{r}/_{2b}} + 19.200\left({}^{r}/_{2b}\right) \\
C_3 &= 0.2020 - 54.620\sqrt{{}^{r}/_{2b}} - 54.748\left({}^{r}/_{2b}\right) \\
C_4 &= 3.232 - 32.530\sqrt{{}^{r}/_{2b}} + 30.964\left({}^{r}/_{2b}\right)
\end{aligned}
\tag{4.23}
$$

4.2.2 Anisotropic Plate

Lekhnitskii (1968) developed a closed-form solution to accurately represent the stresses at any point on an anisotropic plate containing an elliptical cutout. His solution is only intended for in-plane loads that result in an average stress through the thickness of a plate. To satisfy the intent of the solution, any laminate considered for analysis must be symmetric in its stack-up. An unsymmetric laminate will result in out-of-plane bending, which causes stresses not accounted for in the Lekhnitskii solution.

The solution is mathematically intensive and involves complex variables and a complex potential function. This will only be explained on a high level, and if the reader should require more understanding, they are encouraged to review Lekhnitskii's formal write-up (1968).

A stress function, *F(x,y)* as shown in Eq. 4.24, is introduced to satisfy the equilibrium equation.

$$
\sigma_x = \frac{\partial^2 F}{\partial y^2}, \quad \sigma_y = \frac{\partial^2 F}{\partial x^2}, \quad \tau_{xy} = -\frac{\partial^2 F}{\partial x \partial y} \tag{4.24}
$$

A 4th-order differential equation is obtained by substituting Eq. 4.24 into the equilibrium equation.

$$a_{22}\frac{\partial^4 F}{\partial x^4} - 2a_{26}\frac{\partial^4 F}{\partial x^3 \partial y} + \left(2a_{12} + a_{66}\right)\frac{\partial^4 F}{\partial x^2 \partial y^2} - 2a_{16}\frac{\partial^4 F}{\partial x \partial y^3} + a_{11}\frac{\partial^4 F}{\partial y^4} = 0 \qquad (4.25)$$

The a_{ij} coefficients are taken from the inverse-ABD matrix. These coefficients relate the plate stresses directly to the laminate properties. Lekhnitskii showed that Eq. 4.25 could be transferred to four linear operators of the first order D_k.

$$D_1 D_2 D_3 D_4 F(x,y) = 0, \quad D_k = \frac{\partial}{\partial y} - \mu_k \frac{\partial}{\partial x} \qquad (4.26)$$

Eq. 4.25 transforms into a characteristic equation, Eq. 4.27, and μ_k represents four distinct roots. Only the principle roots are used to determine the stress distribution within the plate. The principal roots are the roots that have a result containing a positive imaginary component.

$$a_{11}\mu^4 - 2a_{16}\mu^3 + \left(2a_{12} + a_{66}\right)\mu^2 - 2a_{26}\mu + a_{22} = 0 \qquad (4.27)$$

In the event that the plate is composed of an isotropic or an orthotropic material, the roots can be directly determined. For an isotropic material, the roots are $i = \sqrt{-1}$. To avoid a numerical singularity the roots must be factored by 1.0001 and 0.9999. Eq. 4.28 shows how to calculate the principal roots for an orthotropic laminate using the effective laminate properties.

$$\mu_1 = \frac{i}{2}\left[\sqrt{\frac{\overline{E}_x}{\overline{G}_{xy}} - 2\overline{\nu}_{xy} + 2\sqrt{\frac{\overline{E}_x}{\overline{E}_y}}} + \sqrt{\frac{\overline{E}_x}{\overline{G}_{xy}} - 2\overline{\nu}_{xy} - 2\sqrt{\frac{\overline{E}_x}{\overline{E}_y}}}\right]$$

$$\mu_2 = \frac{i}{2}\left[\sqrt{\frac{\overline{E}_x}{\overline{G}_{xy}} - 2\overline{\nu}_{xy} + 2\sqrt{\frac{\overline{E}_x}{\overline{E}_y}}} - \sqrt{\frac{\overline{E}_x}{\overline{G}_{xy}} - 2\overline{\nu}_{xy} - 2\sqrt{\frac{\overline{E}_x}{\overline{E}_y}}}\right] \qquad (4.28)$$

For the anisotropic materials a complex root solver must be employed to determine the roots and from there, the principal roots must be selected.

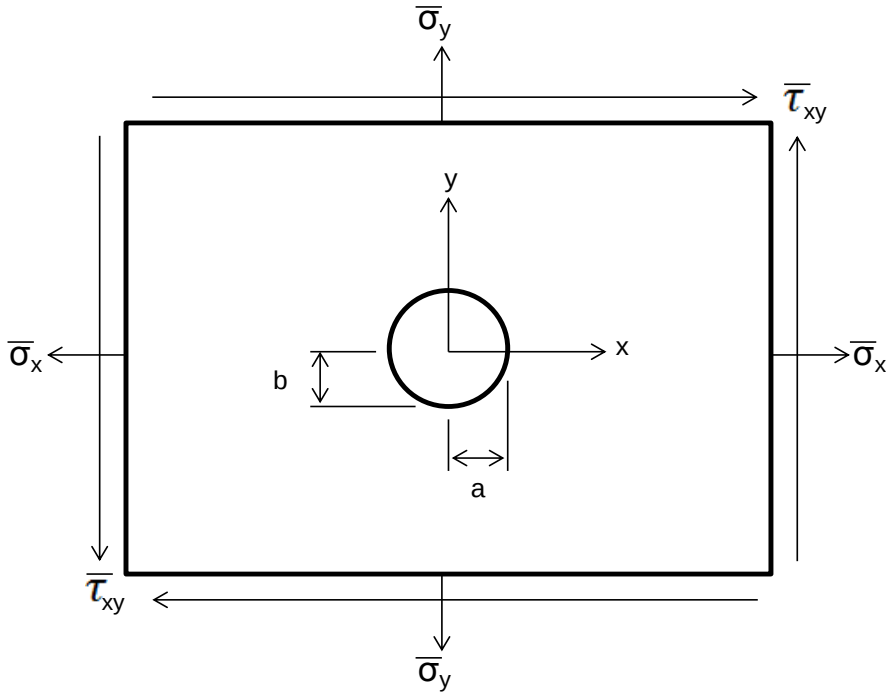

Figure 4.4 Plate Geometry and Loading Configuration

The global x-y coordinates are defined by a complex plane per the following complex variable shown in Eq. 4.29.

$$z_k = x + \mu_k y \qquad (k = 1,2) \tag{4.29}$$

The following mapping function is used to relate the cutout in the x-y plane to a unit circle in the complex plane. For the scenario of a circular cutout, *a* and *b* are equal to radius *R*.

$$z_k = R_k\left(\zeta_k + \frac{t_k}{\zeta_k}\right) \qquad (k = 1,2)$$

$$R_k = \frac{a - i\mu_k b}{2} \tag{4.30}$$

$$t_k = \frac{a + i\mu_k b}{a - i\mu_k b}$$

The inverse mapping function is then defined to be as follows.

$$\zeta_k = \frac{z_k \pm \sqrt{z_k^2 - a^2 - \mu_k^2 b^2}}{a - i\mu_k b} \tag{4.31}$$

Since the inverse mapping function is multi-valued, the correct sign must be found from the following equation.

$$\left|\zeta_k\right| \geq 1 \tag{4.32}$$

Therefore the updated mapping function may be defined using S to represent the correct sign.

$$\zeta_k = \frac{z_k + S\sqrt{z_k^2 - a^2 - \mu_k^2 b^2}}{a - i\mu_k b} \tag{4.33}$$

Using the inverse mapping function, the complex potential functions are as follows.

$$\begin{aligned} C_1 &= \frac{\beta_1 - \mu_2\alpha_1}{\mu_1 - \mu_2} \qquad \varphi_1(z_1) = C_1\frac{1}{\zeta_1} \\ C_2 &= -\frac{\beta_1 - \mu_1\alpha_1}{\mu_1 - \mu_2} \qquad \varphi_2(z_2) = C_2\frac{1}{\zeta_2} \end{aligned} \tag{4.34}$$

$$\alpha_1 = -\frac{\overline{\sigma}_y}{2}a + \frac{\overline{\tau}_{xy}}{2}ib \qquad \beta_1 = -\frac{\overline{\sigma}_x}{2}ib + \frac{\overline{\tau}_{xy}}{2}a \tag{4.35}$$

The derivative of the complex potential function is shown below.

$$\begin{aligned} \varphi'_1(z_1) &= -C_1\left[\frac{z_1 + S\sqrt{z_1^2 - a^2 - \mu_1^2 b^2}}{a - i\mu_1 b}\right]^{-2}\left[\left(1 + \frac{z_1}{S\sqrt{z_1^2 - a^2 - \mu_1^2 b^2}}\right)\frac{1}{a - i\mu_1 b}\right] \\ \varphi'_2(z_2) &= -C_2\left[\frac{z_2 + S\sqrt{z_2^2 - a^2 - \mu_2^2 b^2}}{a - i\mu_2 b}\right]^{-2}\left[\left(1 + \frac{z_2}{S\sqrt{z_2^2 - a^2 - \mu_2^2 b^2}}\right)\frac{1}{a - i\mu_2 b}\right] \end{aligned} \tag{4.36}$$

The stresses at any location on the plate can now be determined using the following equations.

$$\sigma_x^* = 2\,\mathrm{Re}\left[\mu_1^2\varphi'_1(z_1) + \mu_2^2\varphi'_2(z_2)\right] + \bar{\sigma}_x$$

$$\sigma_y^* = 2\,\mathrm{Re}\left[\varphi'_1(z_1) + \varphi'_2(z_2)\right] + \bar{\sigma}_y \qquad (4.37)$$

$$\tau_{xy}^* = -2\,\mathrm{Re}\left[\mu_1\varphi'_1(z_1) + \mu_2\varphi'_2(z_2)\right] + \bar{\tau}_{xy}$$

A Mathcad template can be found in Appendix A.1 to determine the stresses around a circular cutout for an anisotropic laminate. The template produces a diagram and a table populated with results calculated at per degree around the cutout, as seen below.

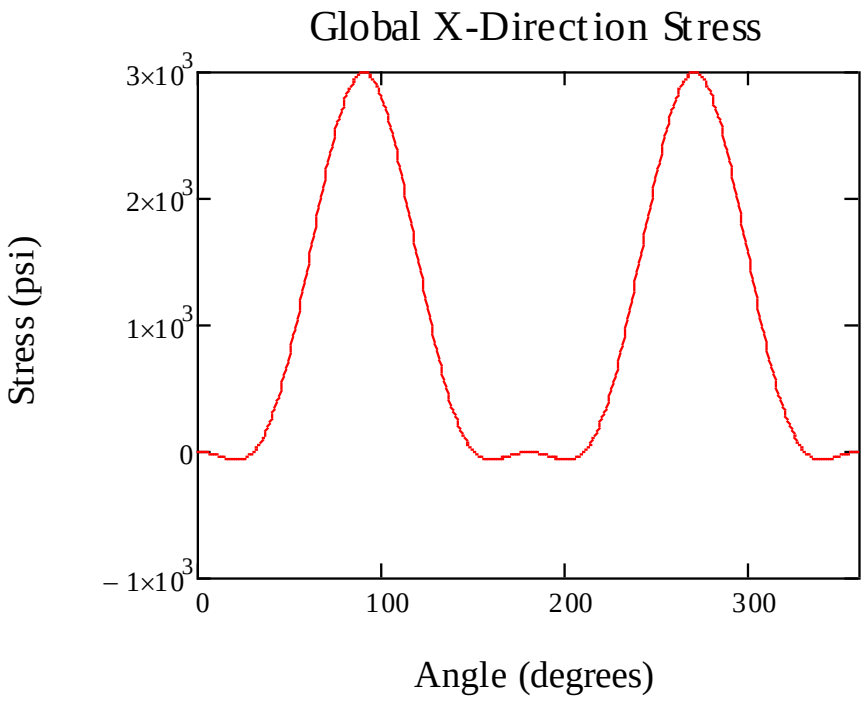

Figure 4.5 Global X-Direction Stress Along Cutout Boundary $[0/\pm45/90]_s$

Table 4.1 Global X-Direction Stress Along Cutout Boundary $[0/\pm45/90]_s$

Angle (deg)	Stress (psi)
0	-0.1
1	-0.403
2	-1.309
3	-2.802
4	-4.859
5	-7.446
6	-10.52
7	-14.032
8	-17.919
9	-22.114
10	-26.54
11	-31.114
12	-35.745
13	-40.335
14	-44.781
15	-48.975
16	-52.804
17	-56.15
18	-58.893
19	-60.91
20	-62.076
21	-62.264
22	-61.35
23	-59.206
24	-55.708
25	-50.733
26	-44.161
27	-35.875
28	-25.764
29	-13.719
30	0.36
31	16.57
32	34.999
33	55.726
34	78.825
35	104.359
36	132.382
37	162.938
38	196.062
39	231.776
40	270.094
41	311.015
42	354.531
43	400.617
44	449.242
45	500.358
46	553.908
47	609.822
48	668.019
49	728.406
50	790.879
51	855.321
52	921.608
53	9.90E+02
54	1.06E+03
55	1.13E+03
56	1.20E+03
57	1.28E+03
58	1.35E+03
59	1.43E+03
60	1.50E+03

Angle (deg)	Stress (psi)
61	1.58E+03
62	1.65E+03
63	1.73E+03
64	1.80E+03
65	1.88E+03
66	1.95E+03
67	2.02E+03
68	2.10E+03
69	2.17E+03
70	2.24E+03
71	2.30E+03
72	2.37E+03
73	2.43E+03
74	2.49E+03
75	2.55E+03
76	2.60E+03
77	2.66E+03
78	2.70E+03
79	2.75E+03
80	2.79E+03
81	2.83E+03
82	2.87E+03
83	2.90E+03
84	2.92E+03
85	2.95E+03
86	2.97E+03
87	2.98E+03
88	2.99E+03
89	3.00E+03
90	3.00E+03
91	3.00E+03
92	2.99E+03
93	2.98E+03
94	2.97E+03
95	2.95E+03
96	2.92E+03
97	2.90E+03
98	2.87E+03
99	2.83E+03
100	2.79E+03
101	2.75E+03
102	2.70E+03
103	2.66E+03
104	2.60E+03
105	2.55E+03
106	2.49E+03
107	2.43E+03
108	2.37E+03
109	2.30E+03
110	2.24E+03
111	2.17E+03
112	2.10E+03
113	2.02E+03
114	1.95E+03
115	1.88E+03
116	1.80E+03
117	1.73E+03
118	1.65E+03
119	1.58E+03
120	1.50E+03

Angle (deg)	Stress (psi)
121	1.43E+03
122	1.35E+03
123	1.28E+03
124	1.20E+03
125	1.13E+03
126	1.06E+03
127	9.90E+02
128	921.608
129	855.321
130	790.879
131	728.406
132	668.019
133	609.822
134	553.908
135	500.358
136	449.242
137	400.617
138	354.531
139	311.015
140	270.094
141	231.776
142	196.062
143	162.938
144	132.382
145	104.359
146	78.825
147	55.726
148	34.999
149	16.57
150	0.36
151	-13.719
152	-25.764
153	-35.875
154	-44.161
155	-50.733
156	-55.708
157	-59.206
158	-61.35
159	-62.264
160	-62.076
161	-60.91
162	-58.893
163	-56.15
164	-52.804
165	-48.975
166	-44.781
167	-40.335
168	-35.745
169	-31.114
170	-26.54
171	-22.114
172	-17.919
173	-14.032
174	-10.52
175	-7.446
176	-4.859
177	-2.802
178	-1.309
179	-0.403
180	-0.1

Rezaeepazhand et al (2005) found that a mapping function could be applied to the Lekhnitskii solution to represent a wider variety of shapes beyond circles and ellipses. Eq. 4.38 was used to create shapes with multiple sides.

$$x = \lambda(\cos\theta)$$
$$y = \lambda(c\sin\theta) \tag{4.38}$$

The λ factor is used to establish the size of the cutout, measuring from the center to the corner. The *w* factor is used to increase or decrease the radius at the corners. The *n* factor is used to establish the number of sides on the cutout. The *c* factor is used to set the length to width ratio. The following figures show how the cutout would be represented in the calculations. Notice how the applied load must be rotated so that it is parallel and perpendicular to the cutout edges.

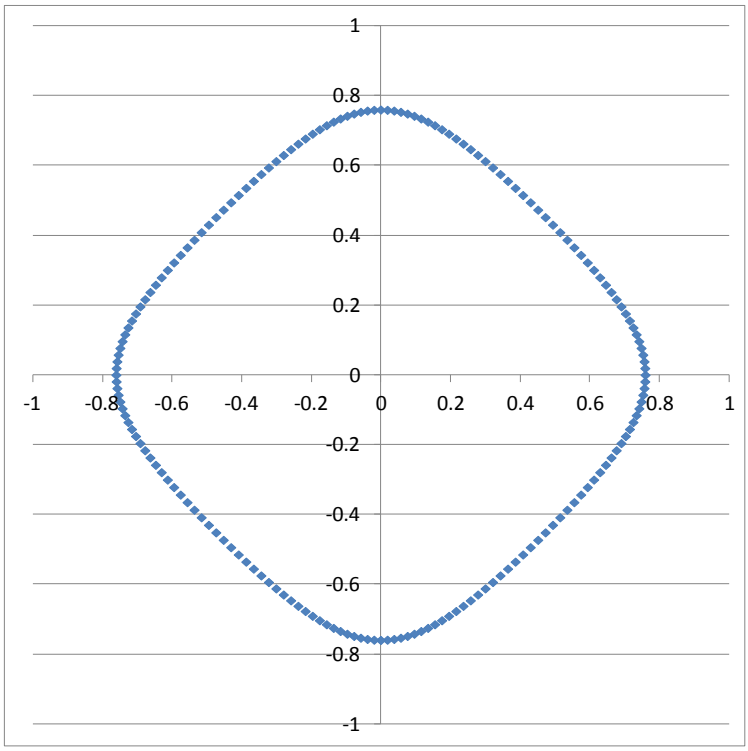

Figure 4.6 Mapping Function – Square (λ=0.707, w=0.075, n=3, c=1)

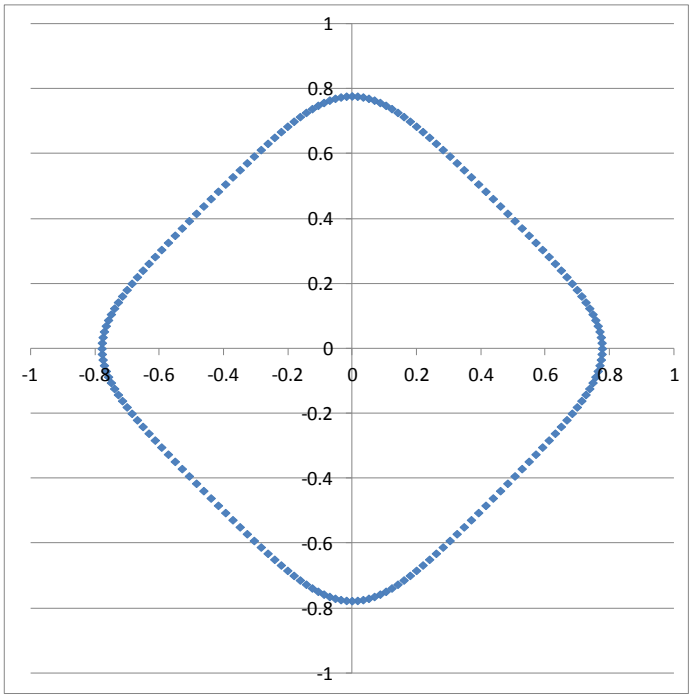

Figure 4.7 Mapping Function – Square (λ=0.707, w=0.1, n=3, c=1)

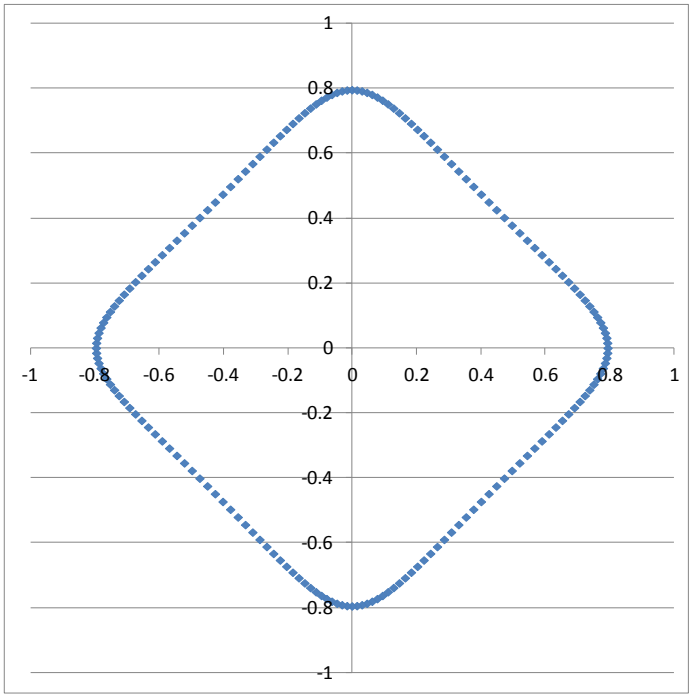

Figure 4.8 Mapping Function – Square (λ=0.707, w=0.125, n=3, c=1)

An attempt was made to integrate the mapping function into the analytical calculations but the results were inconclusive. The majority of the results were plagued by singularities, and the results that did converge could not be correlated with the isotropic solution provided by Sobey. The previous figures display the limited ability to modify the radius of the corners and therefore, the analysis would have been of little value added anyways.

4.3 Laminate Analysis

4.3.1 Circular Cutout

The Lekhnitskii solution was used to calculate the expected SCF for each laminate containing a circular cutout. Composite laminates must maintain strain compatibility through the thickness of the laminate and it cannot be assumed that the angle of maximum principal stress of one ply aligns with each of the others. Therefore, for the analytical and the numerical SCF's, the stress component for the global x-direction, σ_x, was collected and compared to the far-field stress.

Table 4.2 Analytical SCF's for Isotropic Plate and Quasi-Isotropic Laminates

Laminate	**SCF**
Aluminum	3.00
[0/±45/90]s	3.00
[45/0/90/-45]s	3.00

Table 4.3 Analytical SCF's for Orthotropic Laminates

Laminate	**SCF**	**% of 0°**
[±45/90]s	2.33	0
[±45/0]s	3.01	33
[0/±45/0]s	3.28	43
[0/±45/0]s	3.49	50
[45/0/-45/0]s	3.49	50

Table 4.4 Analytical SCF's for Symmetric Anisotropic Laminates

Laminate	SCF	% of 0°
[45/0/90]s	3.51	33
[0/45/90]s	3.51	33
[45/0/$\overline{90}$]s	3.66	40
[45/0]s	4.12	50
[0/45/0/45/0]	4.39	60

As was previously stated, the Lekhnitskii solution is only intended to be used with symmetric laminates in order to avoid the out-of-plane loads. Therefore the results from the Lekhnitskii solution for unsymmetric laminates are of no use in their raw form. They were gathered for observational purposes only and in no way do they alone represent a realistic SCF. The following table presents the results that occurred from the solution.

Table 4.5 Analytical SCF's for Unsymmetric Anisotropic Laminates

Laminate	SCF	% of 0°
[45/45/0/-45/-45]	3.48	20
[0/±45/90]	2.70	25
[0/±45/90]2n	2.92	25
[45/0/90/-45]	3.54	25
[0/45/90]	2.99	33
[0/45/90]2n	3.38	33
[45/45/0/0/-45/-45]	4.01	33
[±45/0]	2.87	33
[0/0/45/45/90/90]	2.99	33
[45/0/90/0/-45]	4.07	40
[0/±45/0/±45/0]	3.32	43
[45/0]2n	4.03	50
[45/0/-45/0]	3.94	50
[45/0/0/-45]	4.55	50
[0/±45/0]	3.71	50
[0/45/0/-45/0]	4.25	60

CHAPTER 5

NUMERICAL RESULTS

This chapter discusses the stresses that were gathered from the finite element models and how they were processed to determine the critical SCF's.

5.1 Lekhnitskii Validation

The Lekhnitskii solution was used in the previous chapter to calculate the SCF's along the boundary of a circular cutout. The following tables show a comparison of the analytical and the numerical results for the circular cutout. Some discrepancy will exist between the two because the Lekhnitskii solution calculates the SCF at the boundary edge, while NASTRAN produces results based on the center of the element in question. Therefore, the first row of elements is essentially producing a stress offset of 0.005" for a 0.01"x0.01" element.

Table 5.1 Symmetric Laminates – Analytical and Numerical SCF's for Circular Cutout

		Analytical	**Numerical**	**Error**
Laminate	**% of 0°**	(Lekhnitskii)	(FEM)	
$[\pm 45/90]_S$	0	2.33	2.33	-0.19%
$[0/\pm 45/90]_S$	25	3.00	2.98	0.67%
$[45/0/90/-45]_S$	25	3.00	2.98	0.67%
$[\pm 45/0]_S$	33	3.01	3.01	0.23%
$[45/0/90]_S$	33	3.51	3.45	1.69%
$[0/45/\overline{90}]_S$	33	3.51	3.45	1.69%
$[45/0/\overline{90}]_S$	40	3.66	3.60	1.74%
$[0/\pm 45/\overline{0}]_S$	43	3.28	3.26	0.61%
$[0/\pm 45/0]_S$	50	3.49	3.46	0.99%
$[45/0/-45/0]_S$	50	3.49	3.46	0.99%
$[45/0]_S$	50	4.12	4.03	2.15%
$[0/45/0/45/0]_T$	60	4.39	4.27	2.77%

Since NASTRAN outputs the stresses in the 1-2 plane, the σ_x had to be determined using the transformation matrix explained in Chapter 4 and then each of the σ_x values for a particular element were averaged together.

The quasi-isotropic and orthotropic laminates achieved nearly perfect correlation but the symmetric anisotropic correlation resulted in a small error percentage. This is believed to be caused by the twisting that comes from an unbalanced laminate.

The comparison between the analytical and numerical results for the unsymmetric laminates turned out just as predicted in Chapter 4. The discrepancy is very large and this is assumed to be due to the out-of-plane bending that results from the unsymmetric laminates.

Table 5.2 Unsymmetric Laminates – Analytical and Numerical SCF's for Circular Cutout

Laminate	% of 0°	Analytical (Lekhnitskii)	Numerical (FEM)	Error
$[45/45/0/-45/-45]_T$	20	3.48	2.55	36.29%
$[0/\pm45/90]_T$	25	2.70	2.78	-2.80%
$[0/\pm45/90]_{2T}$	25	2.92	2.95	-1.02%
$[45/0/90/-45]_T$	25	3.54	2.65	33.85%
$[0/45/90]_T$	33	2.99	3.37	-11.17%
$[0/45/90]_{2T}$	33	3.38	3.42	-1.26%
$[45/45/0/0/-45/-45]_T$	33	4.01	3.00	33.47%
$[\pm45/0]_T$	33	2.87	2.93	-2.17%
$[0/0/45/45/90/90]_T$	33	2.99	3.38	-11.57%
$[45/0/90/0/-45]_T$	40	4.07	3.27	24.52%
$[0/\pm45/0/\pm45/0]_T$	43	3.32	2.81	18.12%
$[45/0]_{2T}$	50	4.03	4.00	0.73%
$[45/0/-45/0]_T$	50	3.94	3.51	12.44%
$[45/0/0/-45]_T$	50	4.55	3.57	27.17%
$[0/\pm45/0]_T$	50	3.71	3.47	6.88%
$[0/45/0/-45/0]_T$	60	4.25	3.82	11.21%

5.2 Laminate Based Stress Concentration Factors

The following tables and diagrams provide the SCF's on the laminate level for the numerical analysis of each of the laminates in combination with each of the cutouts.

5.2.1 Results – Circular Cutout

The following tables are a collection of the peak SCF's for the circular cutout. Since this is a circular cutout, the references to the corners simply represent the quadrants of the circle.

Table 5.3 Laminate SCF – Circular – Symmetric Laminates

		Max SCF per Corner @ 0.005"				MAX SCF
Laminate	**% of 0°**	UL	UR	LL	LR	
$[\pm 45/90]_S$	0	2.33	2.33	2.33	2.33	2.33
$[0/\pm 45/90]_S$	25	2.98	2.98	2.98	2.98	2.98
$[45/0/90/-45]_S$	25	2.98	2.98	2.98	2.98	2.98
$[\pm 45/0]_S$	33	3.00	3.01	3.01	3.01	3.01
$[45/0/90]_S$	33	3.45	3.29	3.29	3.45	3.45
$[0/45/90]_S$	33	3.45	3.29	3.29	3.45	3.45
$[45/0/\overline{90}]_S$	40	3.60	3.45	3.45	3.60	3.60
$[0/\pm 45/\overline{0}]_S$	43	3.26	3.26	3.26	3.26	3.26
$[0/\pm 45/0]_S$	50	3.46	3.46	3.46	3.46	3.46
$[45/0/-45/0]_S$	50	3.46	3.46	3.46	3.46	3.46
$[45/0]_S$	50	4.03	3.97	3.97	4.03	4.03
$[0/45/0/45/0]_T$	60	4.27	4.23	4.23	4.27	4.27

Table 5.4 Laminate SCF – Circular – Unsymmetric Laminates

		Max SCF per Corner @ 0.005"				MAX SCF
Laminate	**% of 0°**	UL	UR	LL	LR	
$[45/45/0/-45/-45]_T$	20	2.55	2.55	2.55	2.55	2.55
$[0/\pm 45/90]_T$	25	2.78	2.75	2.75	2.78	2.78
$[0/\pm 45/90]_{2T}$	25	2.95	2.95	2.95	2.95	2.95
$[45/0/90/-45]_T$	25	2.65	2.64	2.64	2.65	2.65
$[0/45/90]_T$	33	3.36	3.28	3.28	3.37	3.37
$[0/45/90]_{2T}$	33	3.42	3.30	3.30	3.42	3.42
$[45/45/0/0/-45/-45]_T$	33	3.00	3.00	3.00	3.00	3.00
$[\pm 45/0]_T$	33	2.86	2.93	2.93	2.86	2.93
$[0/0/45/45/90/90]_T$	33	3.38	3.31	3.31	3.38	3.38
$[45/0/90/0/-45]_T$	40	3.27	3.27	3.27	3.27	3.27
$[0/\pm 45/0/\pm 45/0]_T$	43	2.79	2.81	2.81	2.79	2.81
$[45/0]_{2T}$	50	4.00	3.96	3.96	4.00	4.00
$[45/0/-45/0]_T$	50	3.48	3.51	3.51	3.48	3.51
$[45/0/0/-45]_T$	50	3.57	3.57	3.57	3.57	3.57
$[0/\pm 45/0]_T$	50	3.47	3.47	3.47	3.47	3.47
$[0/45/0/-45/0]_T$	60	3.82	3.82	3.82	3.82	3.82

5.2.2 Results – Square Cutout with Corner Radius of 0.4 inches

The following tables are a collection of the peak SCF's for the square cutout with corner radii of 0.4 inches.

Table 5.5 Laminate SCF – Square (R=0.4") – Symmetric Laminates

		Max SCF per Corner @ 0.005"				MAX SCF
Laminate	**% of 0°**	UL	UR	LL	LR	
$[\pm 45/90]_S$	0	2.47	2.47	2.47	2.47	2.47
$[0/\pm 45/90]_S$	25	2.97	2.96	2.97	2.97	2.97
$[45/0/90/-45]_S$	25	2.97	2.96	2.97	2.97	2.97
$[\pm 45/0]_S$	33	3.07	3.07	3.07	3.07	3.07
$[45/0/90]_S$	33	3.64	2.88	2.88	3.64	3.64
$[0/45/90]_S$	33	3.64	2.88	2.88	3.64	3.64
$[45/0/\overline{90}]_S$	40	3.75	3.01	3.01	3.76	3.76
$[0/\pm 45/\overline{0}]_S$	43	3.24	3.24	3.24	3.24	3.24
$[0/\pm 45/0]_S$	50	3.38	3.38	3.38	3.38	3.38
$[45/0/-45/0]_S$	50	3.38	3.38	3.38	3.38	3.38
$[45/0]_S$	50	3.96	3.51	3.51	3.96	3.96
$[0/45/0/45/0]_T$	60	4.08	3.69	3.69	4.08	4.08

Table 5.6 Laminate SCF – Square (R=0.4") – Unsymmetric Laminates

		Max SCF per Corner @ 0.005"				MAX SCF
Laminate	**% of 0°**	UL	UR	LL	LR	
$[45/45/0/-45/-45]_T$	20	2.59	2.59	2.59	2.59	2.59
$[0/\pm 45/90]_T$	25	2.85	2.65	2.65	2.85	2.85
$[0/\pm 45/90]_{2T}$	25	2.95	2.92	2.92	2.95	2.95
$[45/0/90/-45]_T$	25	2.64	2.53	2.53	2.64	2.64
$[0/45/90]_T$	33	3.50	2.87	2.87	3.49	3.50
$[0/45/90]_{2T}$	33	3.58	2.89	2.89	3.58	3.58
$[45/45/0/0/-45/-45]_T$	33	2.92	2.92	2.92	2.92	2.92
$[\pm 45/0]_T$	33	2.56	3.04	3.05	2.56	3.05
$[0/0/45/45/90/90]_T$	33	3.48	2.88	2.88	3.48	3.48
$[45/0/90/0/-45]_T$	40	3.06	3.06	3.06	3.06	3.06
$[0/\pm 45/0/\pm 45/0]_T$	43	3.24	3.23	3.24	3.24	3.24
$[45/0]_{2T}$	50	3.86	3.51	3.51	3.86	3.86
$[45/0/-45/0]_T$	50	3.15	3.43	3.44	3.15	3.44
$[45/0/0/-45]_T$	50	3.34	3.33	3.33	3.33	3.34
$[0/\pm 45/0]_T$	50	3.36	3.36	3.36	3.36	3.36
$[0/45/0/-45/0]_T$	60	3.57	3.56	3.56	3.56	3.57

5.2.3 Results – Square Cutout with Corner Radius of 0.3 inches

The following tables are a collection of the peak SCF's for the square cutout with radii of 0.3 inches.

Table 5.7 Laminate SCF – Square (R=0.3") – Symmetric Laminates

		Max SCF per Corner @ 0.005"				MAX SCF
Laminate	**% of 0°**	UL	UR	LL	LR	
$[\pm 45/90]_S$	0	2.62	2.62	2.62	2.62	2.62
$[0/\pm 45/90]_S$	25	3.13	3.13	3.13	3.13	3.13
$[45/0/90/-45]_S$	25	3.13	3.13	3.13	3.13	3.13
$[\pm 45/0]_S$	33	3.26	3.25	3.25	3.25	3.26
$[45/0/90]_S$	33	3.86	3.01	3.01	3.86	3.86
$[0/45/90]_S$	33	3.86	3.01	3.01	3.86	3.86
$[45/0/90]_S$	40	3.98	3.15	3.15	3.98	3.98
$[0/\pm 45/0]_S$	43	3.43	3.43	3.43	3.43	3.43
$[0/\pm 45/0]_S$	50	3.57	3.57	3.57	3.57	3.57
$[45/0/-45/0]_S$	50	3.57	3.57	3.57	3.57	3.57
$[45/0]_S$	50	4.19	3.67	3.67	4.18	4.19
$[0/45/0/45/0]_T$	60	4.29	3.86	3.86	4.28	4.29

Table 5.8 Laminate SCF – Square (R=0.3") – Unsymmetric Laminates

		Max SCF per Corner @ 0.005"				MAX SCF
Laminate	**% of 0°**	UL	UR	LL	LR	
$[45/45/0/-45/-45]_T$	20	2.76	2.76	2.76	2.76	2.76
$[0/\pm 45/90]_T$	25	3.02	2.81	2.81	3.02	3.02
$[0/\pm 45/90]_{2T}$	25	3.12	3.09	3.09	3.12	3.12
$[45/0/90/-45]_T$	25	2.79	2.66	2.66	2.79	2.79
$[0/45/90]_T$	33	3.72	2.99	2.99	3.71	3.72
$[0/45/90]_{2T}$	33	3.80	3.03	3.03	3.80	3.80
$[45/45/0/0/-45/-45]_T$	33	3.09	3.09	3.09	3.09	3.09
$[\pm 45/0]_T$	33	2.69	3.23	3.22	2.68	3.23
$[0/0/45/45/90/90]_T$	33	3.70	3.01	3.01	3.69	3.70
$[45/0/90/0/-45]_T$	40	3.22	3.21	3.21	3.21	3.22
$[0/\pm 45/0/\pm 45/0]_T$	43	3.42	3.42	3.42	3.42	3.42
$[45/0]_{2T}$	50	4.07	3.67	3.67	4.07	4.07
$[45/0/-45/0]_T$	50	3.31	3.62	3.62	3.31	3.62
$[45/0/0/-45]_T$	50	3.51	3.50	3.50	3.50	3.51
$[0/\pm 45/0]_T$	50	3.55	3.54	3.54	3.54	3.55
$[0/45/0/-45/0]_T$	60	3.75	3.74	3.74	3.74	3.75

5.2.4 Results – Square Cutout with Corner Radius of 0.2 inches

The following tables are a collection of the peak SCF's for the square cutout with radii of 0.2 inches.

Table 5.9 Laminate SCF – Square (R=0.2") – Symmetric Laminates

		Max SCF per Corner @ 0.005"				MAX SCF
Laminate	**% of 0°**	UL	UR	LL	LR	
$[\pm 45/90]_S$	0	2.88	2.88	2.88	2.88	2.88
$[0/\pm 45/90]_S$	25	3.42	3.41	3.41	3.41	3.42
$[45/0/90/-45]_S$	25	3.42	3.41	3.41	3.41	3.42
$[\pm 45/0]_S$	33	3.56	3.56	3.56	3.56	3.56
$[45/0/90]_S$	33	4.20	3.23	3.22	4.19	4.20
$[0/45/90]_S$	33	4.20	3.23	3.22	4.19	4.20
$[45/0/\overline{90}]_S$	40	4.33	3.38	3.37	4.32	4.33
$[0/\pm 45/\overline{0}]_S$	43	3.74	3.74	3.74	3.74	3.74
$[0/\pm 45/0]_S$	50	3.88	3.88	3.87	3.87	3.88
$[45/0/-45/0]_S$	50	3.88	3.88	3.87	3.87	3.88
$[45/0]_S$	50	4.54	3.93	3.92	4.53	4.54
$[0/45/0/45/0]_T$	60	4.61	4.12	4.11	4.62	4.62

Table 5.10 Laminate SCF – Square (R=0.2") – Unsymmetric Laminates

		Max SCF per Corner @ 0.005"				MAX SCF
Laminate	**% of 0°**	UL	UR	LL	LR	
$[45/45/0/-45/-45]_T$	20	3.03	3.03	3.03	3.03	3.03
$[0/\pm 45/90]_T$	25	3.29	3.07	3.07	3.29	3.29
$[0/\pm 45/90]_{2T}$	25	3.41	3.36	3.36	3.40	3.41
$[45/0/90/-45]_T$	25	3.04	2.89	2.88	3.04	3.04
$[0/45/90]_T$	33	4.07	3.21	3.20	4.07	4.07
$[0/45/90]_{2T}$	33	4.14	3.25	3.24	4.13	4.14
$[45/45/0/0/-45/-45]_T$	33	3.37	3.37	3.36	3.37	3.37
$[\pm 45/0]_T$	33	2.88	3.53	3.52	2.89	3.53
$[0/0/45/45/90/90]_T$	33	4.04	3.22	3.21	4.04	4.04
$[45/0/90/0/-45]_T$	40	3.47	3.47	3.46	3.47	3.47
$[0/\pm 45/0/\pm 45/0]_T$	43	3.74	3.73	3.73	3.73	3.74
$[45/0]_{2T}$	50	4.40	3.93	3.92	4.40	4.40
$[45/0/-45/0]_T$	50	3.56	3.93	3.92	3.57	3.93
$[45/0/0/-45]_T$	50	3.79	3.79	3.78	3.79	3.79
$[0/\pm 45/0]_T$	50	3.84	3.84	3.84	3.84	3.84
$[0/45/0/-45/0]_T$	60	4.04	4.04	4.03	4.04	4.04

5.2.5 Results – Square Cutout with Corner Radius of 0.1 inches

The following tables are a collection of the peak SCF's for the square cutout with corner radii of 0.1 inches.

Table 5.11 Laminate SCF – Square (R=0.1") – Symmetric Laminates

		Max SCF per Corner @ 0.005"				MAX SCF
Laminate	**% of 0°**	UL	UR	LL	LR	
$[\pm 45/90]_S$	0	3.40	3.39	3.40	3.39	3.40
$[0/\pm 45/90]_S$	25	3.96	3.94	3.95	3.95	3.96
$[45/0/90/-45]_S$	25	3.96	3.94	3.95	3.95	3.96
$[\pm 45/0]_S$	33	4.15	4.13	4.14	4.14	4.15
$[45/0/90]_S$	33	4.83	3.66	3.66	4.80	4.83
$[0/45/90]_S$	33	4.83	3.66	3.66	4.80	4.83
$[45/0/90]_S$	40	4.96	3.82	3.82	4.94	4.96
$[0/\pm 45/0]_S$	43	4.33	4.31	4.32	4.31	4.33
$[0/\pm 45/0]_S$	50	4.45	4.43	4.44	4.44	4.45
$[45/0/-45/0]_S$	50	4.45	4.43	4.44	4.44	4.45
$[45/0]_S$	50	5.17	4.41	4.41	5.15	5.17
$[0/45/0/45/0]_T$	60	5.21	4.59	4.59	5.19	5.21

Table 5.12 Laminate SCF – Square (R=0.1") – Unsymmetric Laminates

		Max SCF per Corner @ 0.005"				MAX SCF
Laminate	**% of 0°**	UL	UR	LL	LR	
$[45/45/0/-45/-45]_T$	20	3.62	3.61	3.61	3.61	3.62
$[0/\pm 45/90]_T$	25	3.84	3.59	3.59	3.83	3.84
$[0/\pm 45/90]_{2T}$	25	3.95	3.88	3.89	3.93	3.95
$[45/0/90/-45]_T$	25	3.55	3.35	3.35	3.54	3.55
$[0/45/90]_T$	33	4.75	3.60	3.60	4.73	4.75
$[0/45/90]_{2T}$	33	4.77	3.67	3.67	4.75	4.77
$[45/45/0/0/-45/-45]_T$	33	3.94	3.92	3.93	3.92	3.94
$[\pm 45/0]_T$	33	3.31	4.10	4.11	3.31	4.11
$[0/0/45/45/90/90]_T$	33	4.70	3.61	3.61	4.69	4.70
$[45/0/90/0/-45]_T$	40	3.94	3.93	3.93	3.93	3.94
$[0/\pm 45/0/\pm 45/0]_T$	43	4.32	4.30	4.31	4.30	4.32
$[45/0]_{2T}$	50	5.02	4.40	4.41	5.00	5.02
$[45/0/-45/0]_T$	50	4.05	4.48	4.49	4.04	4.49
$[45/0/0/-45]_T$	50	4.30	4.28	4.28	4.29	4.30
$[0/\pm 45/0]_T$	50	4.41	4.39	4.40	4.39	4.41
$[0/45/0/-45/0]_T$	60	4.57	4.54	4.54	4.55	4.57

5.2.6 Summary of Cutouts

The results of the laminate based SCF's were divided into family style categories based on the laminate stack-ups.

5.2.6.1 Quasi-Isotropic Results

The quasi-isotropic results are shown in the following table and the isotropic curve is also displayed for comparison purposes. While the SCF's for the smaller radius' did not correlate as well, the curve does show a similar pattern of decreasing SCF until an inflection point where the SCF increases to the value observed for a circular cutout. This is as expected since a quasi-isotropic plate has effective laminate properties that mirror an isotropic plate.

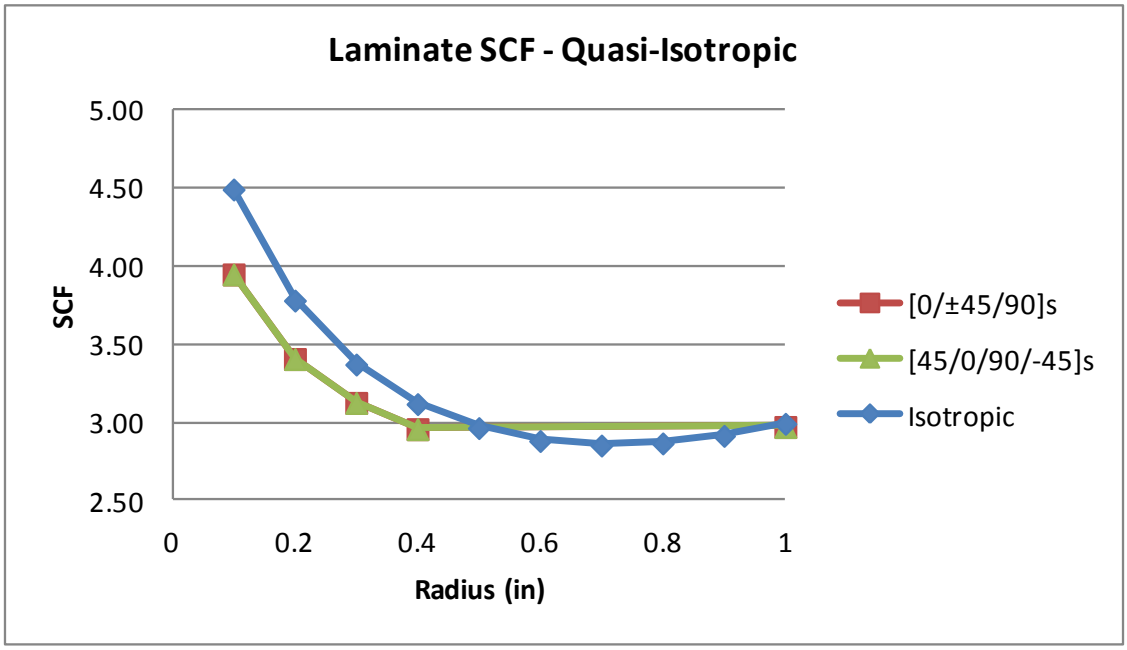

Figure 5.1 Laminate SCF – Quasi-Isotropic Laminates

5.2.6.2 Orthotropic Results

Most of the orthotropic laminates produced results that followed a similar pattern to the quasi-isotropic laminates, as shown in Figure 5.2. The SCF decreased as the corner radius increased, up until an undefined inflection point, where the SCF increased to the value observed for the circular cutout.

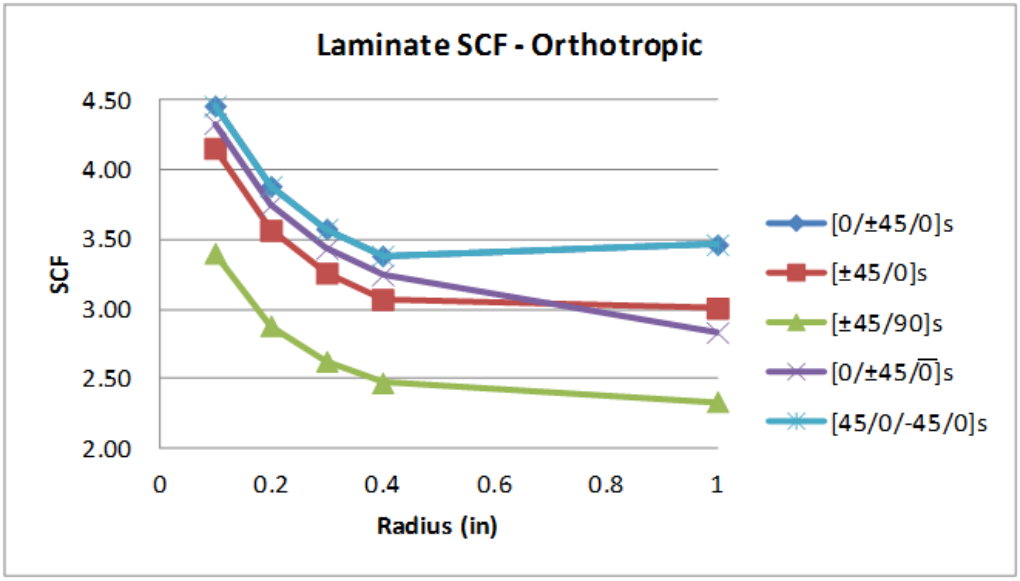

Figure 5.2 Laminate SCF – Orthotropic Laminates

The $[0/\pm45/\bar{0}]_s$ is within the grouping of the majority of the laminates until the shape approaches the circular cutout. The only difference between $[0/\pm45/\bar{0}]_s$ and $[\pm45/0]_s$ is the lower number of 0° plies in the latter. This shows that the slightly lesser stiffness has a more significant impact on the square cutouts than it does the circular cutout.

The $[\pm45/90]_s$ laminate has a significantly lower SCF than the other orthotropic laminates and this can be attributed to the 90° ply located at the mid-plane. The 90° ply lowers the laminate stiffness in the axial direction and therefore creates a softer load path that can absorb the load around the cutout with a limited amount of peaking.

5.2.6.3 Symmetric Anisotropic Results

The symmetric anisotropic results for the laminates without any 90° plies produced similar results to those of similar stack-ups in the orthotropic category. However, the unbalanced effect of the laminates results in a twisting and causes one corner to load up more than the other, as can be seen in the tables previously displayed in this chapter.

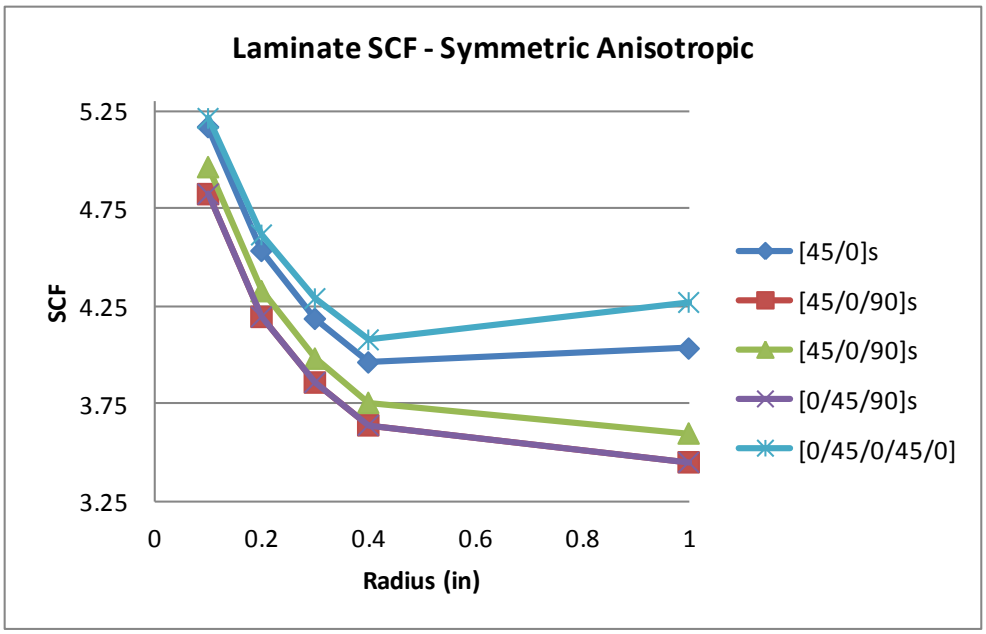

Figure 5.3 Laminate SCF – Symmetric Anisotropic Laminates

All of the symmetric anisotropic laminates that had a 90° ply also had a continuously decreasing SCF, even as the cutout approached the circular shape. As with the orthotropic laminates, the results suggest that the decreased stiffness also relieves the SCF throughout the spectrum of cutouts.

The three laminates with the lowest SCF's on the diagram above are all very similar in their stack-up. As stated in the previous section, the decrease in the SCF's for each cutout for the two lowest laminates is driven by the decrease in stiffness, which is associated with the additional 90° ply in the stack-up.

5.2.6.4 Unsymmetric Anisotropic Results

The unsymmetric anisotropic laminates were divided into two categories. The first group is composed of several laminates that are simply unsymmetric.

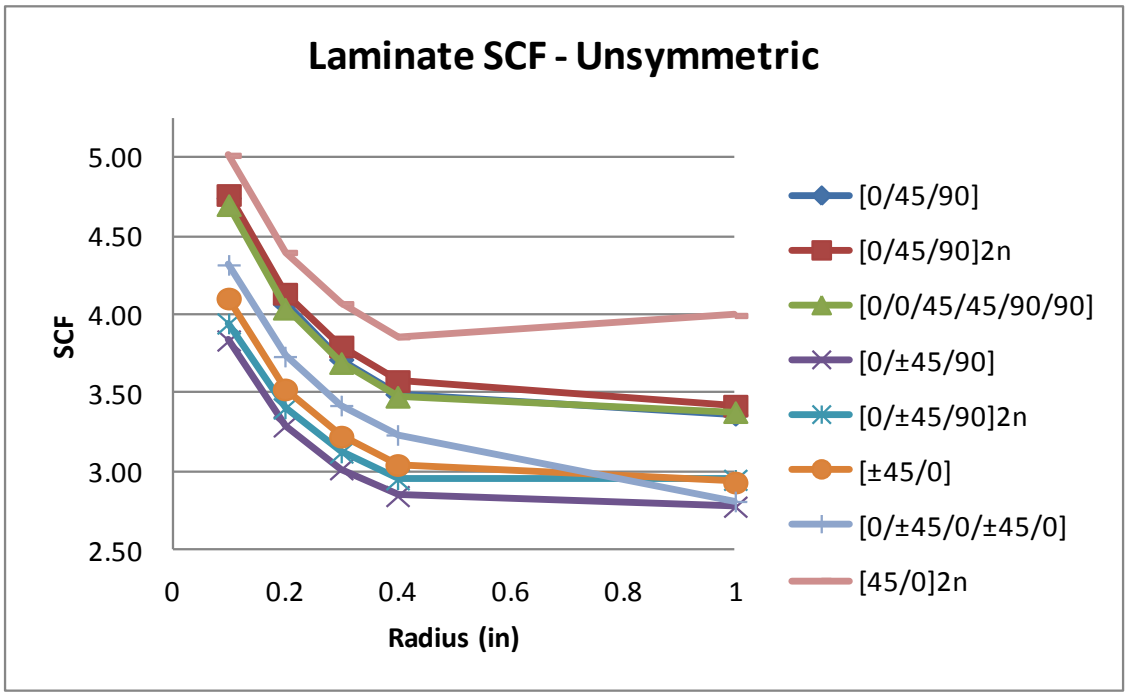

Figure 5.4 Laminate SCF – Unsymmetric Laminates

The $[0/45/90]_T$ and the $[0/0/45/45/90/90]_T$ are essentially identical except in the sense that that the latter is twice the thickness. Since these laminates are unbalanced and unsymmetric, even an axial load results in out-of-plane deflections. The thickness of the $[0/0/45/45/90/90]_T$ laminate may only be twice as thick as $[0/45/90]_T$, but the deflections are reduced by a factor of four.

The unsymmetric and balanced laminates actually resulted in reasonable SCF's that are comparable to the quasi-isotropic laminates and at times, less than the quasi-isotropic laminates.

The second group of unsymmetric anisotropic laminates is composed of antisymmetric or nearly antisymmetric laminates. All of the laminates display results that show that the SCF curves reach lower values than the circular cutout or at least the curves show signs that would prove this had more data points been provided between the radii of 0.4 inches and 1.0 inch.

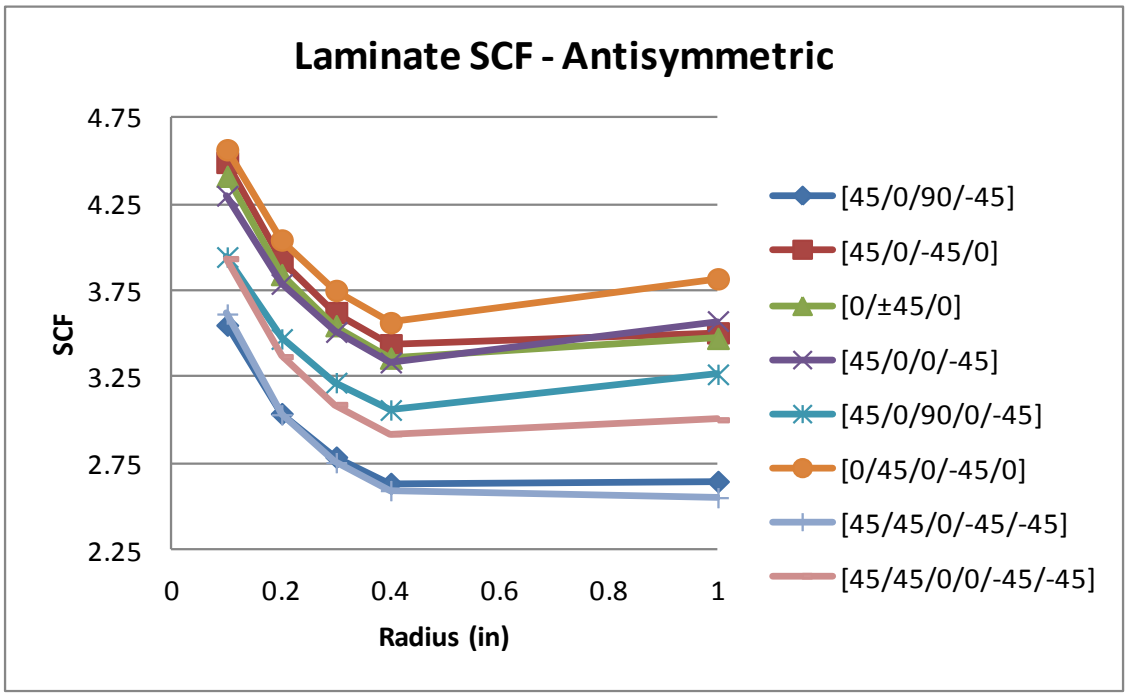

Figure 5.5 Laminate SCF – Antisymmetric Laminates

All of the antisymmetric laminates show reasonable behavior in regards to the SCF curves and also the displacements. The last two curves on the diagram showed a promising pattern of SCF's that appear consistently more advantageous than an isotropic plate, although their stiffness is also lower than that of the quasi-isotropic laminate.

5.3 Lamina Based Stress Concentration Factors – Fiber Stress

The individual ply stresses can provide a great deal of detail as to what is occurring at the micro-level in a laminate. When obtaining the stresses, it is not necessary to reference the global x-y coordinate. The ply properties and capabilities are based upon the individual ply 1-2 plane. Therefore, all ply stresses reported will be the fiber stress in the local coordinate system, unless stated otherwise.

The peak fiber stress is expected to be higher than the peak laminate stress since a laminate stress is an average of all of the plies at a particular location. The SCF based on fiber stress is intended to highlight the spike that a lamina must be capable of sustaining. The peak laminate SCF will be included for comparison.

The fiber stress will also be affected by the out-of-plane deflection that occurs in the unsymmetric laminates but those effects will not be considered in this study. The laminate would need to be supported to prevent any deflection, which would be a plane strain scenario instead of the current plane stress scenario.

5.3.1 Results – Circular Cutout

The following tables are a collection of the peak SCF's for the circular cutout. Since this is a circular cutout, the references to the corners simply represent the quadrants of the circle.

Table 5.13 Lamina SCF – Circular – Symmetric Laminates

		Max SCF per Corner @ 0.005"				Lamina	Laminate	SCF
Laminate	**% of 0°**	UL	UR	LL	LR	MAX SCF	MAX SCF	Ratio
$[\pm45/90]_S$	0	6.19	6.19	6.19	6.19	6.19	2.33	2.65
$[0/\pm45/90]_S$	25	7.52	7.52	7.52	7.52	7.52	2.98	2.53
$[45/0/90/-45]_S$	25	7.52	7.52	7.52	7.52	7.52	2.98	2.53
$[\pm45/0]_S$	33	6.69	6.69	6.69	6.69	6.69	3.01	2.22
$[45/0/90]_S$	33	8.05	8.02	8.02	8.05	8.05	3.45	2.33
$[0/45/90]_S$	33	8.05	8.02	8.02	8.05	8.05	3.45	2.33
$[45/0/\overline{90}]_S$	40	7.30	7.28	7.28	7.30	7.30	3.60	2.03
$[0/\pm45/\overline{0}]_S$	43	6.14	6.14	6.14	6.14	6.14	3.26	1.88
$[0/\pm45/0]_S$	50	5.85	5.85	5.85	5.85	5.85	3.46	1.69
$[45/0/-45/0]_S$	50	5.85	5.85	5.85	5.85	5.85	3.46	1.69
$[45/0]_S$	50	7.03	7.04	7.04	7.03	7.04	4.03	1.74
$[0/45/0/45/0]_T$	60	6.45	6.46	6.46	6.45	6.46	4.27	1.51

Table 5.14 Lamina SCF – Circular – Unsymmetric Laminates

		Max SCF per Corner @ 0.005"				Lamina	Laminate	SCF
Laminate	**% of 0°**	UL	UR	LL	LR	MAX SCF	MAX SCF	Ratio
$[45/45/0/-45/-45]_T$	20	8.32	8.32	8.32	8.32	8.32	2.55	3.26
$[0/\pm45/90]_T$	25	5.31	6.52	6.52	5.31	6.52	2.78	2.35
$[0/\pm45/90]_{2T}$	25	8.51	8.52	8.52	8.51	8.52	2.95	2.89
$[45/0/90/-45]_T$	25	7.51	7.48	7.48	7.51	7.51	2.65	2.84
$[0/45/90]_T$	33	6.04	6.04	6.04	6.04	6.04	3.37	1.80
$[0/45/90]_{2T}$	33	7.91	7.87	7.87	7.92	7.92	3.42	2.31
$[45/45/0/0/-45/-45]_T$	33	7.16	7.16	7.16	7.16	7.16	3.00	2.38
$[\pm45/0]_T$	33	5.25	5.34	5.34	5.25	5.34	2.93	1.82
$[0/0/45/45/90/90]_T$	33	8.17	8.16	8.16	8.17	8.17	3.38	2.42
$[45/0/90/0/-45]_T$	40	6.96	6.96	6.96	6.96	6.96	3.27	2.13
$[0/\pm45/0/\pm45/0]_T$	43	6.16	6.16	6.16	6.16	6.16	2.81	2.19
$[45/0]_{2T}$	50	7.88	7.88	7.88	7.88	7.88	4.00	1.97
$[45/0/-45/0]_T$	50	6.71	6.71	6.71	6.71	6.71	3.51	1.91
$[45/0/0/-45]_T$	50	6.31	6.31	6.31	6.31	6.31	3.57	1.77
$[0/\pm45/0]_T$	50	5.93	5.93	5.93	5.93	5.93	3.47	1.71
$[0/45/0/-45/0]_T$	60	5.73	5.73	5.73	5.73	5.73	3.82	1.50

5.3.2 Results – Square Cutout with Corner Radius of 0.4 inches

The following tables are a collection of the peak SCF's for the square cutout with corner radii of 0.4 inches.

Table 5.15 Lamina SCF – Square (R=0.4") – Symmetric Laminates

		Max SCF per Corner @ 0.005"				Lamina	Laminate	SCF
Laminate	**% of 0°**	UL	UR	LL	LR	MAX SCF	MAX SCF	Ratio
$[\pm45/90]_S$	0	7.70	7.70	7.71	7.70	7.71	2.47	3.12
$[0/\pm45/90]_S$	25	7.42	7.42	7.42	7.42	7.42	2.97	2.50
$[45/0/90/-45]_S$	25	7.42	7.42	7.42	7.42	7.42	2.97	2.50
$[\pm45/0]_S$	33	6.66	6.65	6.66	6.66	6.66	3.07	2.17
$[45/0/90]_S$	33	7.98	7.41	7.41	7.98	7.98	3.64	2.19
$[0/45/90]_S$	33	7.98	7.41	7.41	7.98	7.98	3.64	2.19
$[45/0/\overline{90}]_S$	40	7.13	6.72	6.72	7.13	7.13	3.76	1.90
$[0/\pm45/\overline{0}]_S$	43	6.00	5.99	6.00	5.99	6.00	3.24	1.85
$[0/\pm45/0]_S$	50	5.62	5.62	5.62	5.62	5.62	3.38	1.66
$[45/0/-45/0]_S$	50	5.62	5.62	5.62	5.62	5.62	3.38	1.66
$[45/0]_S$	50	6.44	6.51	6.51	6.44	6.51	3.96	1.64
$[0/45/0/45/0]_T$	60	5.80	5.88	5.88	5.80	5.88	4.08	1.44

Table 5.16 Lamina SCF – Square (R=0.4") – Unsymmetric Laminates

		Max SCF per Corner @ 0.005"				Lamina	Laminate	SCF
Laminate	**% of 0°**	UL	UR	LL	LR	MAX SCF	MAX SCF	Ratio
$[45/45/0/-45/-45]_T$	20	8.24	8.24	8.24	8.24	8.24	2.59	3.18
$[0/\pm45/90]_T$	25	6.77	8.39	8.40	6.78	8.40	2.85	2.95
$[0/\pm45/90]_{2T}$	25	8.43	8.56	8.57	8.43	8.57	2.95	2.90
$[45/0/90/-45]_T$	25	7.33	6.98	6.98	7.33	7.33	2.64	2.78
$[0/45/90]_T$	33	7.13	5.38	5.38	7.14	7.14	3.50	2.04
$[0/45/90]_{2T}$	33	8.14	7.28	7.28	8.14	8.14	3.58	2.27
$[45/45/0/0/-45/-45]_T$	33	6.90	6.90	6.90	6.90	6.90	2.92	2.36
$[\pm45/0]_T$	33	5.69	5.80	5.81	5.68	5.81	3.05	1.91
$[0/0/45/45/90/90]_T$	33	8.94	7.41	7.41	8.94	8.94	3.48	2.57
$[45/0/90/0/-45]_T$	40	6.54	6.54	6.54	6.54	6.54	3.06	2.14
$[0/\pm45/0/\pm45/0]_T$	43	6.00	6.00	6.00	6.00	6.00	3.24	1.86
$[45/0]_{2T}$	50	7.36	7.46	7.47	7.35	7.47	3.86	1.93
$[45/0/-45/0]_T$	50	6.25	6.59	6.59	6.25	6.59	3.44	1.92
$[45/0/0/-45]_T$	50	5.94	5.94	5.94	5.94	5.94	3.34	1.78
$[0/\pm45/0]_T$	50	5.70	5.69	5.69	5.70	5.70	3.36	1.69
$[0/45/0/-45/0]_T$	60	5.40	5.40	5.40	5.40	5.40	3.57	1.52

5.3.3 Results – Square Cutout with Corner Radius of 0.3 inches

The following tables are a collection of the peak SCF's for the square cutout with corner radii of 0.3 inches.

Table 5.17 Lamina SCF – Square (R=0.3") – Symmetric Laminates

		Max SCF per Corner @ 0.005"				Lamina	Laminate	SCF
Laminate	**% of 0°**	UL	UR	LL	LR	MAX SCF	MAX SCF	Ratio
$[\pm 45/90]_S$	0	8.36	8.36	8.36	8.35	8.36	2.62	3.18
$[0/\pm 45/90]_S$	25	7.84	7.83	7.83	7.83	7.84	3.13	2.50
$[45/0/90/-45]_S$	25	7.84	7.83	7.83	7.83	7.84	3.13	2.50
$[\pm 45/0]_S$	33	7.03	7.03	7.02	7.03	7.03	3.26	2.16
$[45/0/90]_S$	33	8.41	7.78	7.78	8.39	8.41	3.86	2.18
$[0/45/90]_S$	33	8.41	7.78	7.78	8.39	8.41	3.86	2.18
$[45/0/\overline{90}]_S$	40	7.51	7.06	7.06	7.49	7.51	3.98	1.89
$[0/\pm 45/\overline{0}]_S$	43	6.32	6.32	6.31	6.32	6.32	3.43	1.84
$[0/\pm 45/0]_S$	50	5.92	5.91	5.91	5.91	5.92	3.57	1.66
$[45/0/-45/0]_S$	50	5.92	5.91	5.91	5.91	5.92	3.57	1.66
$[45/0]_S$	50	6.76	6.83	6.83	6.74	6.83	4.19	1.63
$[0/45/0/45/0]_T$	60	6.07	6.15	6.15	6.05	6.15	4.29	1.43

Table 5.18 Lamina SCF – Square (R=0.3") – Unsymmetric Laminates

		Max SCF per Corner @ 0.005"				Lamina	Laminate	SCF
Laminate	**% of 0°**	UL	UR	LL	LR	MAX SCF	MAX SCF	Ratio
$[45/45/0/-45/-45]_T$	20	8.70	8.70	8.69	8.70	8.70	2.76	3.16
$[0/\pm 45/90]_T$	25	7.39	9.17	9.17	7.39	9.17	3.02	3.04
$[0/\pm 45/90]_{2T}$	25	8.89	9.05	9.04	8.89	9.05	3.12	2.90
$[45/0/90/-45]_T$	25	6.87	6.86	6.85	6.86	6.87	2.79	2.46
$[0/45/90]_T$	33	7.78	5.64	5.64	7.79	7.79	3.72	2.09
$[0/45/90]_{2T}$	33	8.63	7.64	7.63	8.62	8.63	3.80	2.27
$[45/45/0/0/-45/-45]_T$	33	7.28	7.27	7.27	7.27	7.28	3.09	2.36
$[\pm 45/0]_T$	33	6.28	6.33	6.33	6.26	6.33	3.23	1.96
$[0/0/45/45/90/90]_T$	33	9.74	7.75	7.75	9.74	9.74	3.70	2.64
$[45/0/90/0/-45]_T$	40	7.72	7.31	7.31	7.71	7.72	3.22	2.40
$[0/\pm 45/0/\pm 45/0]_T$	43	6.34	6.33	6.32	6.33	6.34	3.42	1.85
$[45/0]_{2T}$	50	7.72	7.85	7.85	7.71	7.85	4.07	1.93
$[45/0/-45/0]_T$	50	6.55	6.95	6.95	6.54	6.95	3.62	1.92
$[45/0/0/-45]_T$	50	6.25	6.24	6.23	6.23	6.25	3.51	1.78
$[0/\pm 45/0]_T$	50	6.02	6.01	6.01	6.01	6.02	3.55	1.70
$[0/45/0/-45/0]_T$	60	5.69	5.68	5.68	5.67	5.69	3.75	1.52

5.3.4 Results – Square Cutout with Corner Radius of 0.2 inches

The following tables are a collection of the peak SCF's for the square cutout with corner radii of 0.2 inches.

Table 5.19 Lamina SCF – Square (R=0.2") – Symmetric Laminates

		Max SCF per Corner @ 0.005"				Lamina	Laminate	SCF
Laminate	**% of 0°**	UL	UR	LL	LR	MAX SCF	MAX SCF	Ratio
$[\pm45/90]_S$	0	9.41	9.40	9.39	9.39	9.41	2.88	3.27
$[0/\pm45/90]_S$	25	8.50	8.50	8.49	8.49	8.50	3.42	2.49
$[45/0/90/-45]_S$	25	8.50	8.50	8.49	8.49	8.50	3.42	2.49
$[\pm45/0]_S$	33	7.64	7.63	7.62	7.63	7.64	3.56	2.14
$[45/0/90]_S$	33	9.08	8.41	8.40	9.09	9.09	4.20	2.16
$[0/45/90]_S$	33	9.08	8.41	8.40	9.09	9.09	4.20	2.16
$[45/0/\overline{90}]_S$	40	8.09	7.63	7.62	8.09	8.09	4.33	1.87
$[0/\pm45/\overline{0}]_S$	43	6.83	6.83	6.82	6.82	6.83	3.74	1.82
$[0/\pm45/0]_S$	50	6.40	6.39	6.39	6.40	6.40	3.88	1.65
$[45/0/-45/0]_S$	50	6.40	6.39	6.39	6.40	6.40	3.88	1.65
$[45/0]_S$	50	7.24	7.36	7.34	7.24	7.36	4.54	1.62
$[0/45/0/45/0]_T$	60	6.47	6.61	6.59	6.48	6.61	4.62	1.43

Table 5.20 Lamina SCF – Square (R=0.2") – Unsymmetric Laminates

		Max SCF per Corner @ 0.005"				Lamina	Laminate	SCF
Laminate	**% of 0°**	UL	UR	LL	LR	MAX SCF	MAX SCF	Ratio
$[45/45/0/-45/-45]_T$	20	9.45	9.44	9.43	9.44	9.45	3.03	3.11
$[0/\pm45/90]_T$	25	8.38	10.37	10.36	8.35	10.37	3.29	3.15
$[0/\pm45/90]_{2T}$	25	9.66	9.85	9.84	9.65	9.85	3.41	2.89
$[45/0/90/-45]_T$	25	8.35	7.86	7.84	8.33	8.35	3.04	2.75
$[0/45/90]_T$	33	8.81	6.05	6.04	8.80	8.81	4.07	2.17
$[0/45/90]_{2T}$	33	9.37	8.23	8.23	9.36	9.37	4.14	2.27
$[45/45/0/0/-45/-45]_T$	33	7.86	7.86	7.85	7.86	7.86	3.37	2.33
$[\pm45/0]_T$	33	7.11	7.18	7.17	7.07	7.18	3.53	2.04
$[0/0/45/45/90/90]_T$	33	10.99	8.34	8.33	10.96	10.99	4.04	2.72
$[45/0/90/0/-45]_T$	40	7.40	7.40	7.39	7.41	7.41	3.47	2.13
$[0/\pm45/0/\pm45/0]_T$	43	6.87	6.86	6.85	6.85	6.87	3.74	1.84
$[45/0]_{2T}$	50	8.30	8.49	8.48	8.30	8.49	4.40	1.93
$[45/0/-45/0]_T$	50	7.02	7.54	7.53	7.02	7.54	3.93	1.92
$[45/0/0/-45]_T$	50	6.71	6.72	6.70	6.72	6.72	3.79	1.77
$[0/\pm45/0]_T$	50	6.50	6.50	6.49	6.51	6.51	3.84	1.69
$[0/45/0/-45/0]_T$	60	6.11	6.11	6.10	6.12	6.12	4.04	1.51

5.3.5 Results – Square Cutout with Corner Radius of 0.1 inches

The following tables are a collection of the peak SCF's for the square cutout with corner radii of 0.1 inches.

Table 5.21 Lamina SCF – Square (R=0.1") – Symmetric Laminates

		Max SCF per Corner @ 0.005"				Lamina	Laminate	SCF
Laminate	**% of 0°**	UL	UR	LL	LR	MAX SCF	MAX SCF	Ratio
$[\pm45/90]_S$	0	11.39	11.42	11.40	11.39	11.42	3.40	3.36
$[0/\pm45/90]_S$	25	9.77	9.73	9.75	9.74	9.77	3.96	2.47
$[45/0/90/-45]_S$	25	9.77	9.73	9.75	9.74	9.77	3.96	2.47
$[\pm45/0]_S$	33	8.73	8.69	8.71	8.70	8.73	4.15	2.10
$[45/0/90]_S$	33	10.26	9.62	9.63	10.23	10.26	4.83	2.13
$[0/45/90]_S$	33	10.26	9.62	9.63	10.23	10.26	4.83	2.13
$[45/0/\overline{90}]_S$	40	9.10	8.70	8.71	9.08	9.10	4.96	1.83
$[0/\pm45/\overline{0}]_S$	43	7.76	7.72	7.74	7.73	7.76	4.33	1.79
$[0/\pm45/0]_S$	50	7.69	7.70	7.70	7.70	7.70	4.45	1.73
$[45/0/-45/0]_S$	50	7.69	7.70	7.70	7.70	7.70	4.45	1.73
$[45/0]_S$	50	8.08	8.26	8.26	8.05	8.26	5.17	1.60
$[0/45/0/45/0]_T$	60	7.19	7.38	7.38	7.17	7.38	5.21	1.42

Table 5.22 Lamina SCF – Square (R=0.1") – Unsymmetric Laminates

		Max SCF per Corner @ 0.005"				Lamina	Laminate	SCF
Laminate	**% of 0°**	UL	UR	LL	LR	MAX SCF	MAX SCF	Ratio
$[45/45/0/-45/-45]_T$	20	10.87	10.82	10.84	10.83	10.87	3.62	3.01
$[0/\pm45/90]_T$	25	10.21	12.66	12.63	10.22	12.66	3.84	3.30
$[0/\pm45/90]_{2T}$	25	11.15	11.37	11.39	11.12	11.39	3.95	2.89
$[45/0/90/-45]_T$	25	9.57	9.73	9.69	9.52	9.73	3.55	2.74
$[0/45/90]_T$	33	10.56	6.81	6.80	10.57	10.57	4.75	2.23
$[0/45/90]_{2T}$	33	12.90	11.33	11.35	12.84	12.90	4.77	2.71
$[45/45/0/0/-45/-45]_T$	33	8.92	8.87	8.89	8.88	8.92	3.94	2.27
$[\pm45/0]_T$	33	8.61	8.77	8.75	8.60	8.77	4.11	2.14
$[0/0/45/45/90/90]_T$	33	13.26	9.41	9.40	13.27	13.27	4.70	2.82
$[45/0/90/0/-45]_T$	40	8.41	8.36	8.38	8.37	8.41	3.94	2.13
$[0/\pm45/0/\pm45/0]_T$	43	7.94	7.94	7.95	7.95	7.95	4.32	1.84
$[45/0]_{2T}$	50	9.33	9.61	9.61	9.31	9.61	5.02	1.92
$[45/0/-45/0]_T$	50	7.98	8.53	8.53	7.94	8.53	4.49	1.90
$[45/0/0/-45]_T$	50	7.55	7.51	7.50	7.53	7.55	4.30	1.76
$[0/\pm45/0]_T$	50	7.43	7.44	7.44	7.44	7.44	4.41	1.69
$[0/45/0/-45/0]_T$	60	7.41	7.41	7.41	7.41	7.41	4.57	1.62

5.3.6 Summary of Cutouts

The results of the lamina based SCF's were divided into the same family style categories that the laminate based SCF's were, which was based on the laminate stack-ups.

An investigation was conducted to survey the particular plies that achieved the peak stress of the laminate at the given offset. As expected, when a 0° ply was present it was nearly always the ply with the peak stress. This is because it has the highest stiffness in the applied load direction. The unsymmetric laminates were the exception to this rule but only for a couple of the laminates. The unsymmetric stack-up changes the center of bending in the laminate and can therefore allow another ply to reach a greater strain and in turn a greater stress.

5.3.6.1 Quasi-Isotropic Results

The quasi-isotropic laminates matched identically to each other as expected. This shows a relatively high stress closest to the edge of the cutout. SCF's that reach such a value suggest the possibility of the edge of the cutout becoming plastic, as Whitney stated.

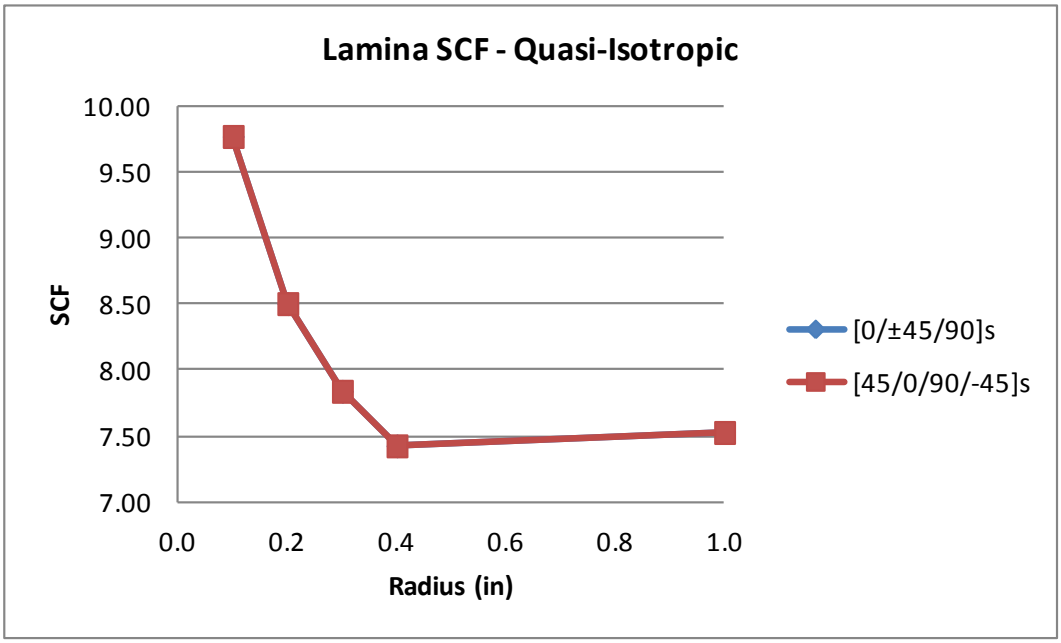

Figure 5.6 Lamina SCF – Quasi-Isotropic Laminates

5.3.6.2 Orthotropic Results

The orthotropic lamina results are in an opposite order or increasing magnitude of that compared to the laminate results. This would suggest that the selection of a laminate stack-up would involve a compromise between max lamina stress and max laminate stress.

A noticeable spike in the $[\pm 45/90]_s$ laminate occurs. Since the laminate does not contain any 0° plies, the 45° plies have the highest stiffness and therefore draw the most load.

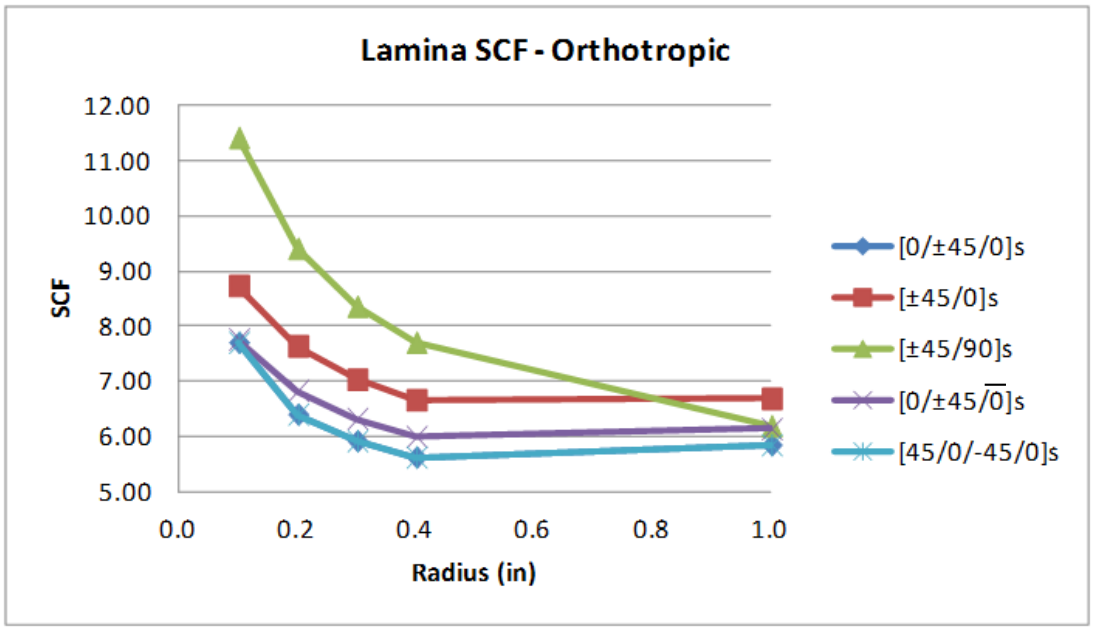

Figure 5.7 Lamina SCF – Orthotropic Laminates

5.3.6.3 Symmetric Anisotropic Results

The symmetric anisotropic results are also in an inverted order of magnitude, just as the orthotropic laminate results. The data shows that it does not matter whether the 0° degree ply is the outer most layer or if it is embedded within the laminate. This is only truly valid for a symmetric laminate because the applied load is distributed evenly between the upper and lower half of the laminate.

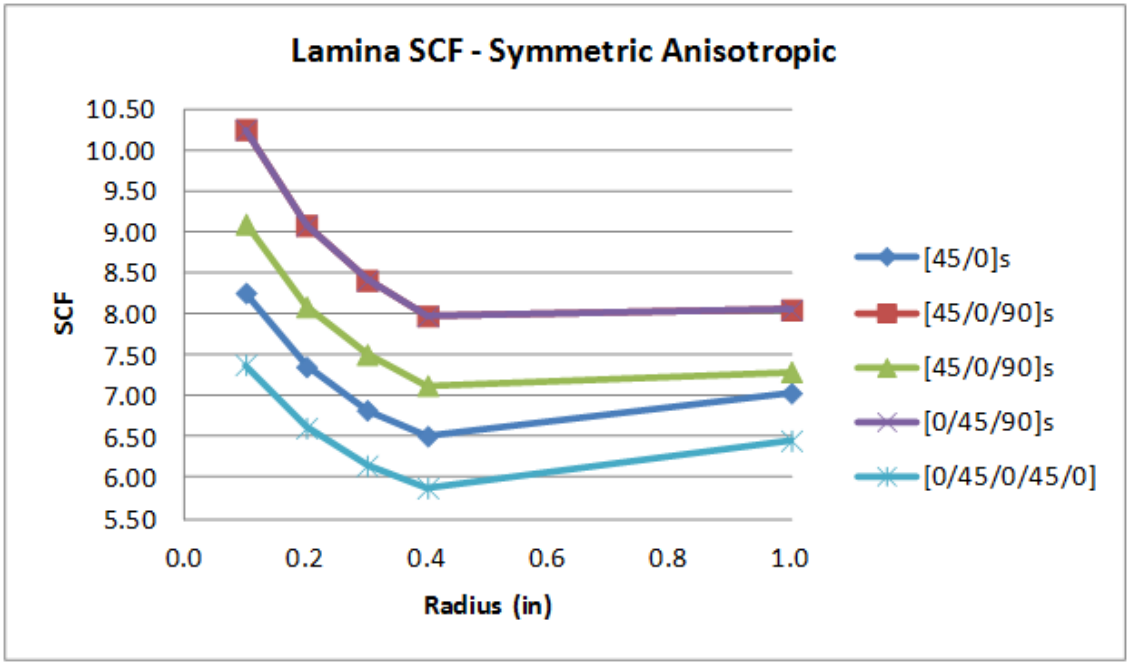

Figure 5.8 Lamina SCF – Symmetric Anisotropic Laminates

5.3.6.4 Unsymmetric Anisotropic Results

Just as with the laminate results, the unsymmetric anisotropic laminates have been divided into two categories. The first group is composed of several laminates that are simply unsymmetric.

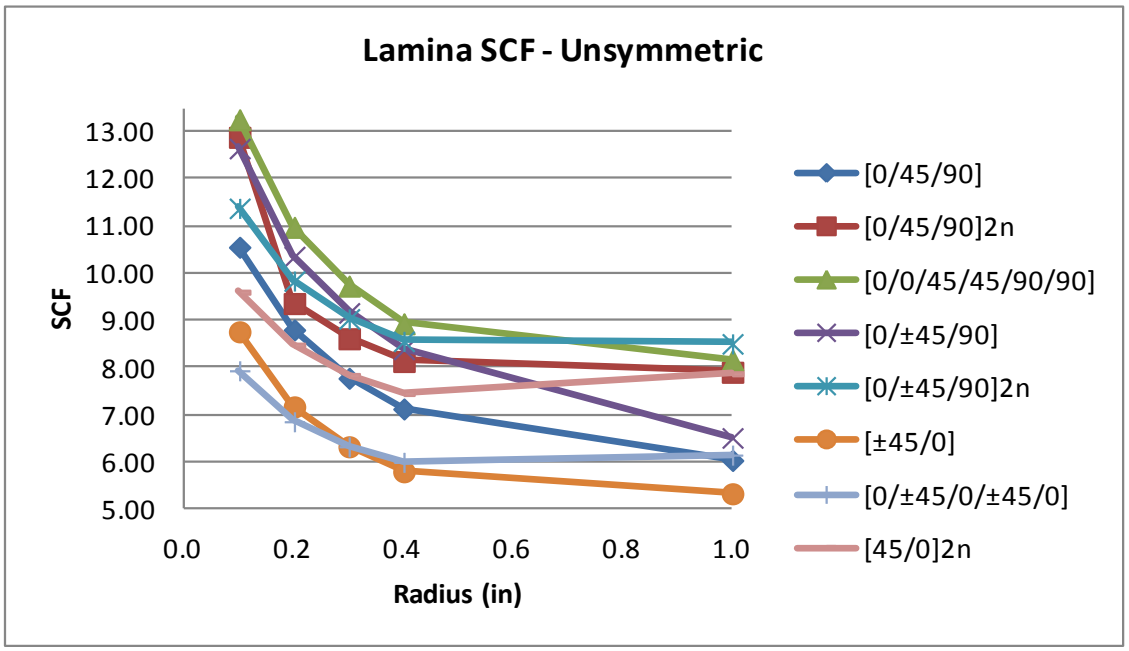

Figure 5.9 Lamina SCF – Unsymmetric Laminates

The $[0/\pm45/0/\pm45/0]_T$ laminate seems to be a very capably candidate for a laminate with a cutout. It results in having near the lowest lamina and laminate SCF's and it is also sufficiently stiff to carry a reasonable amount of load.

The $[0/\pm45/90]_T$ laminate was very promising when considering the laminate SCF but according to the results above the ply stresses are significantly increased for the square cutouts. The circular cutout would still result in a very efficient structure.

The second group of unsymmetric anisotropic results is composed of antisymmetric or nearly antisymmetric laminates. The results are inverted in magnitude just as the symmetric laminates were.

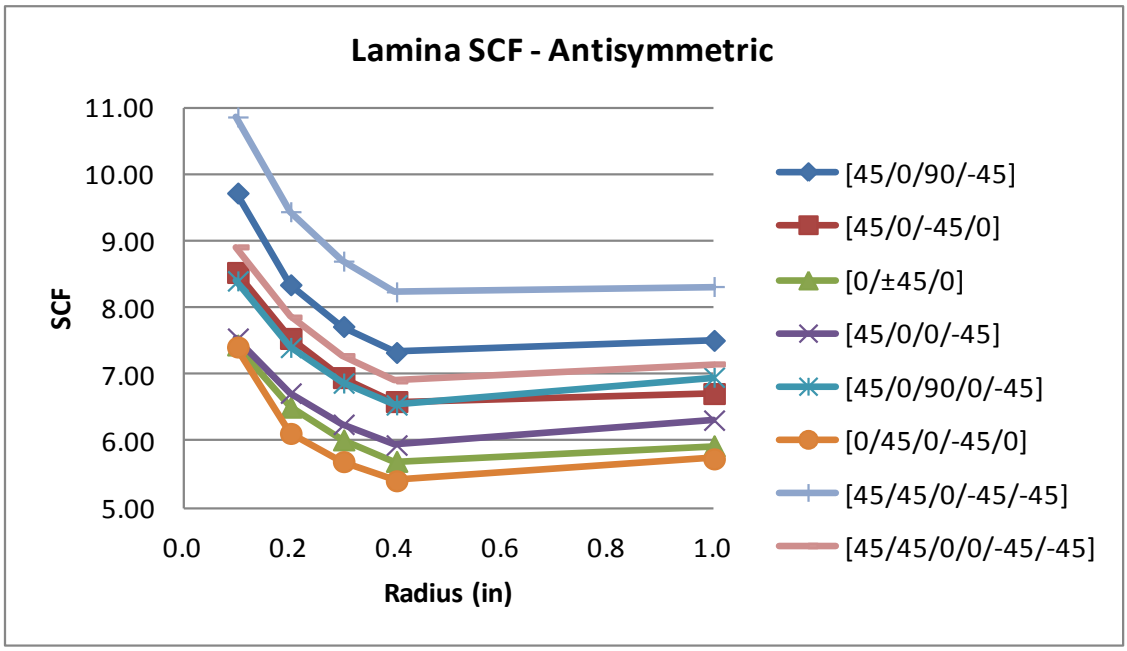

Figure 5.10 Lamina SCF – Antisymmetric Laminates

5.4 Stress Distribution

The rate of stress distribution that diminishes the local SCF can significantly impact the design of the structure. An efficient structure will return the area around the cutout back to the far-field stress levels in the shortest distance possible.

Using the laminate SCF's, the SCF's were plotted versus the offset distance for each fo the cutouts in several of the laminates. The vast majority of the laminates all followed a similar pattern, such as the quasi-isotropic laminate shown below.

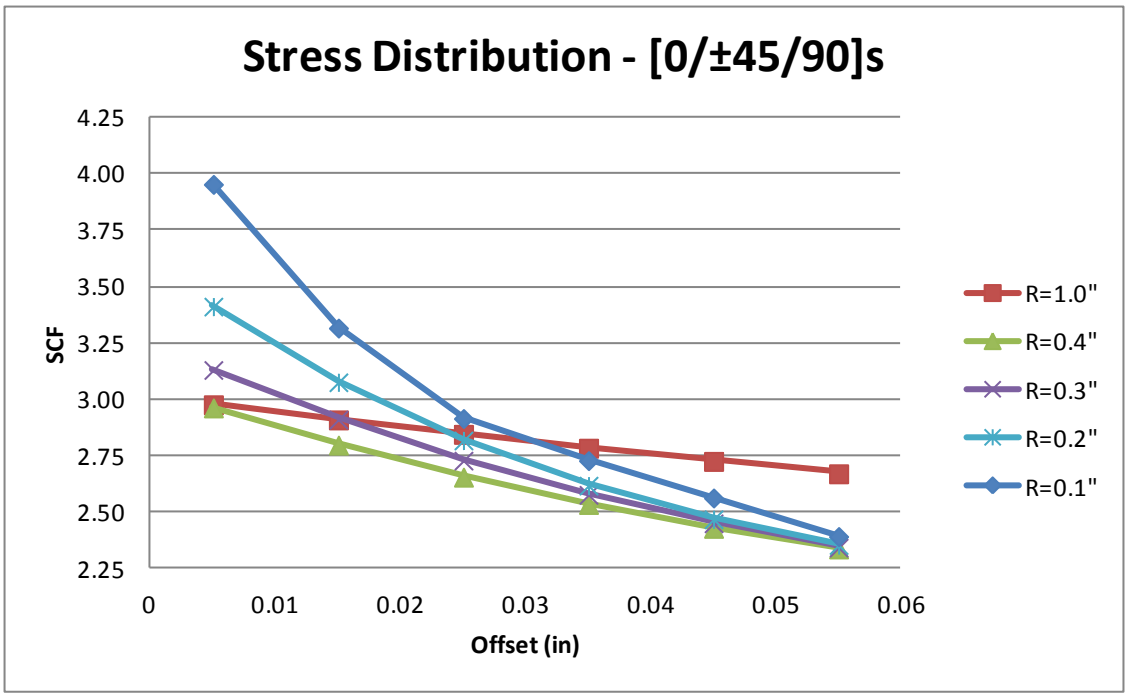

Figure 5.11 Stress Distribution for $[0/\pm45/90]_s$ Laminate

It is common for the square cutouts to have higher SCF's than the circular cutout. As the offset distance increases the SCF's of the square cutout decrease at a higher rate and eventually surpass the SCF of the circular cutout.

However, laminates with a high percentage ±45° plies were unable to get the SCF's of the square cutout to reach the SCF's of the circular cutout or they were at least delayed to a greater off set distance. It is worth noting that the SCF's for this laminate are significantly less than those of an isotropic but this comparison is directly for the cutout shapes of an individual laminate. The trend shows that laminates with a lower stiffness, less 0° plies, distribute the stress over a greater distance.

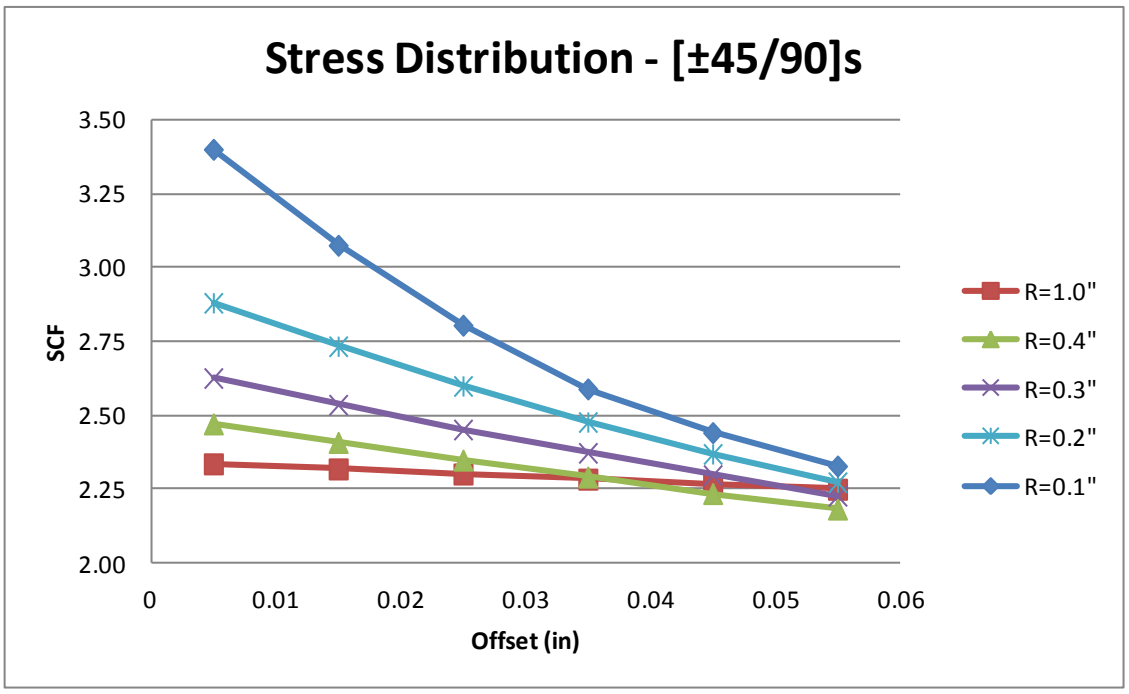

Figure 5.12 Stress Distribution for $[\pm 45/90]_s$ Laminate

The following figure shows that laminates with a higher stiffness, more 0° plies, tend to distribute the stress at an advanced rate for square cutouts.

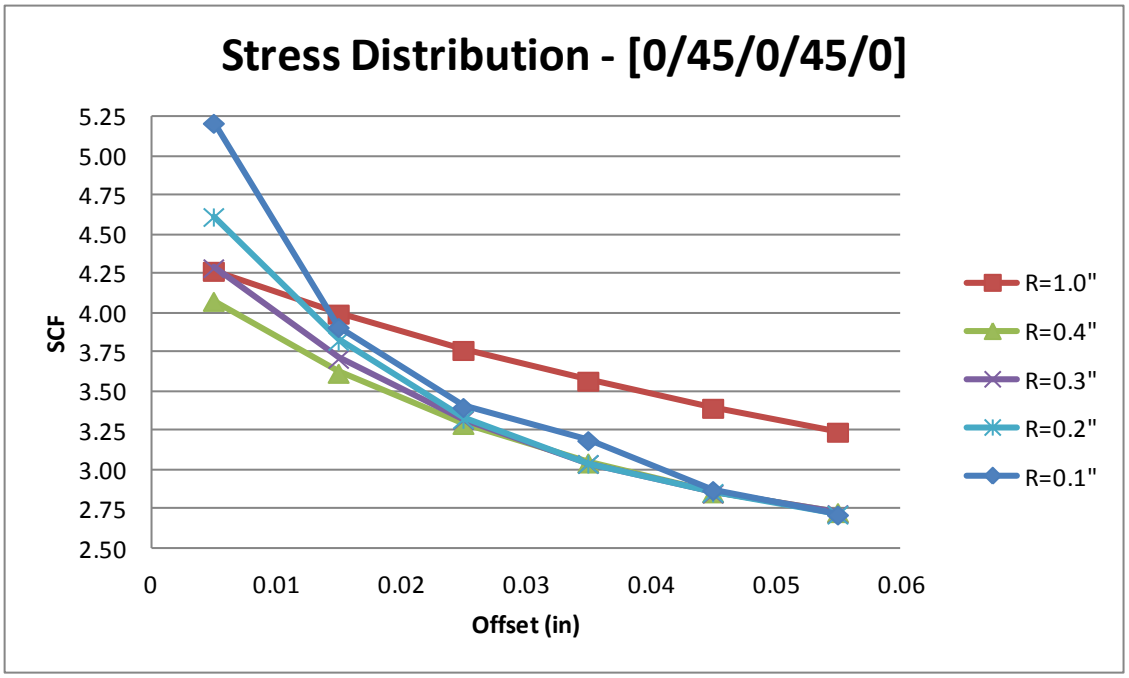

Figure 5.13 Stress Distribution for $[0/45/0/45/0]_T$ Laminate

CHAPTER 6

CONCLUSION

This research has the studied the stress concentration factors that develop in a composite laminate containing a square cutout with rounded corners. Laminates of all varieties, symmetric and balanced to unsymmetric and unbalanced, composed of carbon/epoxy composite were considered for evaluation. The radii at the corners were iterated to determine the effects on the growth of the stress concentration factor and a circular cutout of the same width was evaluated to validate the study. Lekhnitskii's closed-form solution was employed to determine the stresses in an anisotropic plate to validate the stress concentration factors for the circular cutout.

A model was created in PATRAN for each cutout shape and then each model was output to a NASTRAN deck. The NASTRAN decks were populated with each of the laminates to be considered and then the analysis was executed. The resulting stress concentration factors for the circular cutout achieved excellent correlation for the symmetric laminates but it was already known that the Lekhnitskii solution was incapable of determining the stresses for unsymmetric laminates. The stress concentration factors were collected from the NASTRAN results for all cutouts and all laminates.

From this research, the following conclusions can be made:

- The quasi-isotropic laminate results in lower stress concentration factors than the isotropic plate
- Decreasing the percent of 0° plies and/or increasing the percent of 45° plies reduces the stress concentration factors for all cutout shapes

- Laminates with an increased number of 90° plies continuously decreases the stress concentration factor so that the lowest value is achieved for the circular cutout.
- Antisymmetric laminates successfully reduce the stress concentration factor without a significant loss in stiffness or excessive deflection.
- The laminate stress concentration factors and the lamina stress concentration factors show consistent correlation with the SCF ratio.
- Laminates with no 0° plies significantly increase the lamina stresses for the existing laminate.
- The rate of stress distribution can be categorized according to the percent of 0° plies.
- The lower percentage of 0° plies results in a delayed return to the far-field stress.
- The rate of stress distribution increases with laminates that have a greater stiffness.

Going forward, I believe there are still several opportunities to expand on this study. The current mapping function to analyze the square cutout with a closed-form solution is limited to unrealistic shapes. The mapping solution needs to be revisited and modified to take into account a perfect square with rounded corners that can be modified.

The current study needs to be extended by adding data points between the radii of 0.4" and 1.0" to determine the true minimum stress concentration factors for each cutout shape and laminate combination.

APPENDIX A

LEKHNITSKII'S FORMALISM IN A MATHCAD TEMPLATE

The following is an example of the Mathcad template used to evaluate Lekhnitskii's formalism.

$R := 1$

Load Data

$\sigma_X := 1000$

$\sigma_Y := 0$

$\sigma_{XY} := 0$

$a_{11} := 1.279 \times 10^{-6}$ $a_{12} := -8.119 \times 10^{-7}$ $a_{16} := -2.625 \times 10^{-99}$

$a_{22} := 3.747 \times 10^{-6}$ $a_{26} := -2.625 \times 10^{-99}$

$a_{66} := 4.155 \times 10^{-6}$

$p(\mu) := a_{11} \cdot \mu^4 - 2 \cdot a_{16} \cdot \mu^3 + (2 \cdot a_{12} + a_{66}) \cdot \mu^2 - 2 \cdot a_{26} \cdot \mu + a_{22}$

$$v := p(\mu)\ \text{coeffs} \rightarrow \begin{pmatrix} 0.000003747 \\ 5.25e\text{-}99 \\ 0.0000025312 \\ 5.25e\text{-}99 \\ 0.000001279 \end{pmatrix}$$

$r := \text{polyroots}(v)$

$$r = \begin{pmatrix} -0.601 - 1.162i \\ -0.601 + 1.162i \\ 0.601 - 1.162i \\ 0.601 + 1.162i \end{pmatrix}$$

Principal roots are those that have a positive imaginary component.

$r_1 = -0.601 + 1.162i$ $\mu_1 := r_1 = -0.601 + 1.162i$

$r_3 = 0.601 + 1.162i$ $\mu_2 := r_3 = 0.601 + 1.162i$

$$\alpha_1 := \frac{-\sigma_Y}{2}\cdot R + \frac{\sigma_{XY}}{2}\cdot i\cdot R$$

$$\beta_1 := \left(\frac{-\sigma_X}{2}\cdot i\cdot R\right) + \frac{\sigma_{XY}}{2}\cdot R$$

$$C1 := \frac{\beta_1 - \mu_2\cdot\alpha_1}{\mu_1 - \mu_2} \qquad C2 := -\left(\frac{\beta_1 - \mu_1\cdot\alpha_1}{\mu_1 - \mu_2}\right)$$

$$S_1(z_1) := \begin{cases} 1 & \text{if } \left|\frac{(z_1) + \sqrt{(z_1)^2 - R^2 - {\mu_1}^2\cdot R^2}}{R - i\cdot\mu_1\cdot R}\right| \geq 1 \\ -1 & \text{otherwise} \end{cases}$$

$$S_2(z_2) := \begin{cases} 1 & \text{if } \left|\frac{(z_2) + \sqrt{(z_2)^2 - R^2 - {\mu_2}^2\cdot R^2}}{R - i\cdot\mu_2\cdot R}\right| \geq 1 \\ -1 & \text{otherwise} \end{cases}$$

$$\phi_{prime1}(z_1) := C1\cdot\left[-1\cdot\left[\frac{(z_1) + S_1(z_1)\cdot\sqrt{(z_1)^2 - R^2 - {\mu_1}^2\cdot R^2}}{R - i\cdot\mu_1\cdot R}\right]^{-2}\cdot\left[\left[1 + \frac{S_1(z_1)\cdot(z_1)}{\sqrt{(z_1)^2 - R^2 - {\mu_1}^2\cdot R^2}}\right]\cdot\frac{1}{R - i\cdot\mu_1\cdot R}\right]\right]$$

$$\phi_{prime2}(z_2) := C2\cdot\left[-1\cdot\left[\frac{(z_2) + S_2(z_2)\cdot\sqrt{(z_2)^2 - R^2 - {\mu_2}^2\cdot R^2}}{R - i\cdot\mu_2\cdot R}\right]^{-2}\cdot\left[\left[1 + \frac{S_2(z_2)\cdot(z_2)}{\sqrt{(z_2)^2 - R^2 - {\mu_2}^2\cdot R^2}}\right]\cdot\frac{1}{R - i\cdot\mu_2\cdot R}\right]\right]$$

$$\sigma_x(x,y) := 2\cdot Re\left(\mu_1^{\,2}\cdot\phi_{prime1}\left(x+\mu_1\cdot y\right)+\mu_2^{\,2}\cdot\phi_{prime2}\left(x+\mu_2\cdot y\right)\right)+\sigma_X$$

$$\sigma_y(x,y) := 2\cdot Re\left(\phi_{prime1}\left(x+\mu_1\cdot y\right)+\phi_{prime2}\left(x+\mu_2\cdot y\right)\right)+\sigma_Y$$

$$\sigma_{xy}(x,y) := -2\cdot Re\left(\mu_1\cdot\phi_{prime1}\left(x+\mu_1\cdot y\right)+\mu_2\cdot\phi_{prime2}\left(x+\mu_2\cdot y\right)\right)+\sigma_{XY}$$

$$\sigma_{max}(x,y) := \frac{\left(\sigma_x(x,y)+\sigma_y(x,y)\right)}{2}+\sqrt{\left[\frac{\left(\sigma_x(x,y)-\sigma_y(x,y)\right)}{2}\right]^2+\sigma_{xy}(x,y)^2}$$

$i := 0, 1..360$

$CD := 0.0001$

$x1_i := (R + CD)\cdot\cos(i\cdot deg)$

$y1_i := (R + CD)\cdot\sin(i\cdot deg)$

REFERENCES

1. Merlin, P. W., “Design and Development of the Blackbird: Challenges and Lessons Learned”, AIAA 2009-1522, 2009.
2. The Boeing Co., www.boeing.com, 2012
3. Inglis, C. E., “Stresses in a Plate Due to the Presence of Cracks and Sharp Corners”, Fifty-fourth Session of the Institution of Naval Architects, 1913.
4. Heller, S. R. Jr., Brock, J. S., Bart, R., The Stresses Around a Rectangular Opening with Rounded Corners in a Uniformly Loaded Plate, January 1959.
5. Sobey, A. J., “Stress-Concentration Factors for Rounded Rectangular Holes in Infinite Sheets”, Ministry of Aviation, November 1963.
6. Lekhnitskii, S. G., “Theory of Elasticity of an Anisotropic Body”, Holden-Day, San Francisco, 1968.
7. Lekhnitskii, S. G., “Anisotropic Plates”, Gordon and Breach, 1968.
8. Daniel, I. M., Rowlands, R. E., Whiteside, J. B., “Effects of Material and Stacking Sequence on Behavior of Composite Plates with Holes”, January 1974.
9. Whitney, J. M., Nuismer, R. J., “Stress Fracture Criteria for Laminated Composites Containing Stress Concentrations”, Journal of Composites Materials, July 1974.
10. Konish, H. J., Whitney, J. M., Approximate Stresses in an Orthotropic Plate Containing a Circular Hole”, Journal of Composite Materials, April 1975.
11. Rajaiah, K., Naik, N. K., “Quasi-Rectangular Holes with Minimum Stress Concentrations in Orthotropic Plates”, Journal of Reinforced Plastics and Composites, July 1983.
12. Ko, W. L., “Stress Concentration Around a Small Circular Hole in the HiMAT Composite Plate”, NASA, December 1985.

13. Tan, S. C., “Finite-Width Correction Factors for Anisotropic Plate Containing a Central Opening”, Journal of Composite Materials, November 1988.
14. Rezaeepazhand, J., Jafari, M., “Stress Analysis of Perforated Composite Plates”, Composite Structures, #71, 2005.
15. Rezaeepazhand, J., Jafari, M., “Stress Analysis of Composite Plates with a Quasi-Square Cutout Subjected to Uniaxial Tension”, Journal of Reinforced Plastics and Composites, July 2010.
16. Pilkey, W. D., Pilkey, D. F., “Peterson’s Stress Concentration Factors”, 3rd ed., John Wiley & Sons, Inc., New Jersey, 2008.

BIOGRAPHICAL INFORMATION

Colin Cannon received his Bachelor of Science in Aerospace Engineering from the University of Texas at Arlington in 2007. He was an active member of the student engineering community, spending portions of his undergraduate career with the Formula SAE team, the AIAA student organization, as a lab instructor and also as an intern with Vought Aircraft Industries.

Upon graduation in 2007, Colin began his engineering career with Vought as a design engineer and then quickly transitioned into a stress engineer position. After taking a year off of school, Colin rejoined UTA in 2008 to begin his Master of Science in Aerospace Engineering. His primary focus was structural analysis, with an emphasis on composites.

Colin received his Master's degree in December of 2012 and upon graduation he moved to Colorado and accepted a position with Sierra Nevada Corporation in yet another engineering opportunity.